Pair-truncated shell-model analysis of nuclei around mass 130

Koji Higashiyama[1,*] and Naotaka Yoshinaga[2,†]
[1]*Department of Physics, Chiba Institute of Technology, Narashino, Chiba 275-0023, Japan*
[2]*Department of Physics, Saitama University, Saitama City 338-8570, Japan*
(Received 24 November 2010; revised manuscript received 16 February 2011; published 28 March 2011)

Low-lying states for even-even, odd-mass, and doubly odd nuclei in the mass $A \sim 130$ region are systematically investigated using a pair-truncated shell model. In this model the collective nucleon pairs with angular momenta zero and two are the basic ingredients for even-even nuclei. Additional unpaired nucleons are added to the even-even core for a description of odd-mass and doubly odd nuclei. The effective interactions consist of single-particle energies and monopole and quadrupole pairing plus quadrupole-quadrupole interactions, whose strengths are assumed to be linearly changed as functions of the number of nucleons so as to describe the level schemes of the even-even and odd-mass nuclei. Energy levels of the low-lying collective states for even-even Xe, Ba, Ce, and Nd isotopes are reproduced very well along with intraband and interband $B(E2)$ values, which simulate the typical features of the O(6) limit of the interacting boson model. For odd-mass and doubly odd nuclei, complicated level schemes and electromagnetic moments are in excellent agreement with the experimental data.

DOI: 10.1103/PhysRevC.83.034321 PACS number(s): 21.60.Cs, 21.60.Ev, 27.60.+j

I. INTRODUCTION

The study of nuclei in the mass $A \sim 130$ region which have protons just more than 50 and neutrons just fewer than 82 has been a subject of special interest recently. For instance, even-even nuclei exhibit the γ instability or weak triaxiality in low-lying states, which is characterized by the energy staggering in quasi-γ bands and some forbidden transition rates between yrast and quasi-γ bands. This feature comes from the prolatelike mass distribution of valence proton particles and oblatelike mass distribution of valence neutron holes. In the past three decades, many theoretical studies on these nuclei were carried out through various approaches. A widely used theory for describing the even-even nuclei is the interacting boson model (IBM) [1], where quadrupole collective excitations are described in terms of angular-momenta-zero (s) and -two (d) bosons. The low-lying states of the nuclei in this mass region were extensively investigated within the framework of the IBM, and the energy spectra and electromagnetic transitions were well approximated by the Hamiltonian with O(6) dynamical symmetry [2–12].

The level schemes of odd-mass nuclei in the mass $A \sim 130$ region have quite a complicated structure, which is caused by the interplay between single-particle and collective degrees of freedom. For a description of odd-mass nuclei, the IBM was extended to include the fermionic degree of freedom in addition to the boson core. The extended model, the so-called interacting boson fermion model (IBFM) [13], has been widely used in studies of the odd-mass nuclei in the mass $A \sim 130$ region [14–21]. The simplest version of the IBFM (IBFM-1) was applied to positive- and negative-parity states of the odd-mass Xe and Ba isotopes, and the complicated level schemes and electromagnetic properties were well reproduced [14,15]. Using different sets of single-particle orbitals, similar calculations were carried out for the odd-mass nuclei in this mass region [18–20]. The IBFM-2 distinguishing between neutron bosons and proton bosons has also been successful in describing the low-lying states of the odd-mass nuclei, $_{54}$Xe and $_{55}$Cs isotopes [16,21], and $_{56}$Ba and $_{57}$La isotopes [17].

Recently a new approach has been developed where the bosons are explicitly treated as nucleon collective pairs. The pair-truncated shell model (PTSM) has presented a unified description of quadrupole collective motion and the excitation of single-particle degrees of freedom in medium-heavy nuclei [22–32]. In its simplest version of the PTSM, the full shell-model space is restricted within the SD subspace where angular-momenta-zero (S) and -two (D) collective pairs are used as the building blocks. For a description of odd-mass and doubly odd nuclei, additional unpaired nucleons are added to the even-even nuclear states. Based on this framework, systematic studies were performed on the even-even and odd-mass nuclei in the mass $A \sim 130$ region [28]. This approach reproduced well various properties of Xe, Ba, $_{58}$Ce, and $_{60}$Nd isotopes. The same set of interactions used for even-even nuclei was applied to doubly odd nuclei, and excellent agreement with the experimental data was achieved for both the energy spectra and the electromagnetic properties of the doublet bands with the $\nu h_{11/2} \otimes \pi h_{11/2}$ configuration [30–32]. The theoretical results revealed new aspects of the band structure of the doubly odd nuclei in this mass region. These bands were also investigated in terms of the quadrupole coupling model (QCM) [33–36]. The excitation mechanism predicted by the previous PTSM calculations has again been confirmed in the QCM.

In this paper, we present systematic calculations for the even-even, the odd-mass, and the doubly odd nuclei in the mass $A \sim 130$ region using the SD version of the PTSM. We employ the monopole and quadrupole pairing plus quadrupole-quadrupole interaction as a two-body effective interaction, and take into account all the five $0g_{7/2}$, $1d_{5/2}$, $1d_{3/2}$, $0h_{11/2}$, and $2s_{1/2}$ orbitals in the major shell of $50 \leqslant N\ (Z) \leqslant 82$ for neutrons (protons).

*koji.higashiyama@it-chiba.ac.jp
†yoshinaga@phy.saitama-u.ac.jp

In the previous PTSM study [28], energy spectra of both the yrast and the quasi-γ bands for even-even Xe, Ba, Ce, and Nd isotopes were well reproduced. However, this interaction fails in reproducing the relative spacings between the positive- and negative-parity states for the proton-odd nuclei, Cs and La isotopes. The purpose of the present study is to systematically describe the energy levels and electromagnetic properties for all the even-even, odd-mass, and doubly odd nuclei in the mass $A \sim 130$ region, especially by taking care of the relative spacings between the positive- and negative-parity states for Cs and La isotopes. In order to achieve that purpose, the single-particle energies and the two-body interaction strengths are changed linearly with the number of valence particles to give an improved fitting for odd-mass nuclei.

The paper is organized as follows. In Sec. II, the framework of the PTSM and its form of effective interactions in the model space are presented. In Sec. III the PTSM calculations are carried out for the even-even nuclei, $^{134-126}$Xe, $^{136-128}$Ba, $^{138-130}$Ce, and $^{140-132}$Nd, where the two-body interactions are smoothly changed as functions of valence particles. In Sec. IV we apply the PTSM to odd-mass nuclei, and calculate the energy spectra and the electromagnetic moments for $^{135-129}$Xe, $^{137-131}$Ba, $^{139-133}$Ce, $^{135-129}$Cs, and $^{137-131}$La. In Sec. V energy levels for the low-lying states and electromagnetic moments are given for doubly odd nuclei, ^{132,130}Cs and ^{134,132}La. The principal results are summarized in Sec. VI.

II. THEORETICAL FRAMEWORK

The nuclear shell model remains one of the most fundamental approaches for a microscopic description of nuclear structure. It has been successful for understanding the structure of light nuclei. On the other hand, the model cannot be applied to medium and heavy nuclei except for a few nuclei lying near a shell closure. The main difficulty is the uncontrollable problem of dimension explosion. In order to avoid this problem, we truncate the shell-model subspace to the space that is constructed only in terms of angular-momentum-zero (S) and -two (D) collective pairs. These pairs, as building blocks of the model, are defined as

$$S^\dagger = \sum_j \alpha_j A_0^{\dagger(0)}(jj), \tag{1}$$

$$D_M^\dagger = \sum_{j_1 j_2} \beta_{j_1 j_2} A_M^{\dagger(2)}(j_1 j_2), \tag{2}$$

where α and β are the structure coefficients. Here the creation operator of a nucleon pair with total angular momentum J and its projection M is defined as

$$A_M^{\dagger(J)}(j_1 j_2) = \sum_{m_1 m_2} (j_1 m_1 j_2 m_2 | JM) c_{j_1 m_1}^\dagger c_{j_2 m_2}^\dagger = [c_{j_1}^\dagger c_{j_2}^\dagger]_M^{(J)}, \tag{3}$$

where $(j_1 m_1 j_2 m_2 | JM)$ stands for a Clebsch-Gordan coefficient. Here $c_{jm}^\dagger$ represents either a neutron-hole creation operator or a proton-particle creation operator, and (j, m) represents a set of quantum numbers necessary to specify the state (n, ℓ, j, m). In the mass $A \sim 130$ region we treat neutrons as holes and protons as particles so that $N = 82$ and $Z = 50$ become the nearest closed shells. The S and D pairs are constructed in each neutron or proton space separately.

The structure coefficients α and β are determined so as to maximize the collectivity of the S and D pairs. More explicitly, the structure of the collective S pair is determined by variation,

$$\delta \langle S^n | \hat{H} | S^n \rangle = 0, \tag{4}$$

with $|S^n\rangle = (S^\dagger)^n |-\rangle$, where $|-\rangle$ indicates the closed-shell core, n represents the number of the valence nucleon pairs for a specific nucleus, and $\hat{H}$ is an interaction among like nucleons. In the second step, with use of the S pair obtained above, the structure of the collective D pair is determined by variation,

$$\delta \langle S^{n-1} D | \hat{H} | S^{n-1} D \rangle = 0, \tag{5}$$

with $|S^{n-1} D\rangle = (S^\dagger)^{n-1} D^\dagger |-\rangle$. After determining the structure of the S and D pairs, a many-body SD-pair state of like nucleons is constructed as

$$|S^{n_s} D^{n_d} \eta I\rangle = (S^\dagger)^{n_s} (D^\dagger)^{n_d} |-\rangle, \tag{6}$$

where I is the total angular momentum of the SD-pair state, and η an additional quantum number required to completely specify the state. Here, the angular momentum coupling is carried out exactly, but we abbreviate its notation.

To describe open-shell nuclei, we use the SD-pair states in both neutron and proton spaces, and couple them to the state with a total spin I. Thus the many-body wave function of the even-even nucleus can be written as

$$|\Phi(I\eta)\rangle = [|S^{\bar{n}_s} D^{\bar{n}_d}(I_\nu \eta_\nu)\rangle \otimes |S^{n_s} D^{n_d}(I_\pi \eta_\pi)\rangle]^{(I)}, \tag{7}$$

where $\bar{n}_s$ and $\bar{n}_d$ represent the numbers of neutron-hole S and D pairs, respectively, while n_s and n_d correspond to those for proton-particle pairs. The numbers $2(\bar{n}_s + \bar{n}_d)$ and $2(n_s + n_d)$ are the total number of valence neutron holes $\bar{N}_\nu$ and that of proton particles N_π, respectively. The SD-pair states are generally nonorthogonal to each other and the Schmidt orthogonalization procedure is necessary.

As an effective two-body interaction, we employ the monopole and quadrupole pairing plus quadrupole-quadrupole interaction. The effective shell-model Hamiltonian is written as

$$\hat{H} = \hat{H}_\nu + \hat{H}_\pi + \hat{H}_{\nu\pi}, \tag{8}$$

where $\hat{H}_\nu$, $\hat{H}_\pi$, and $\hat{H}_{\nu\pi}$ represent the interaction among neutrons, the interaction among protons, and the interaction between neutrons and protons, respectively. The interaction among like nucleons $\hat{H}_\tau$ ($\tau = \nu$ or π) consists of spherical single-particle energies, monopole pairing (MP) interaction, quadrupole-pairing (QP) interaction, and quadrupole-quadrupole (QQ) interaction,

$$\hat{H}_\tau = \sum_{jm} \varepsilon_{j\tau} c_{jm\tau}^\dagger c_{jm\tau} - G_{0\tau} \hat{P}_\tau^{\dagger(0)} \hat{P}_\tau^{(0)} - G_{2\tau} \hat{P}_\tau^{\dagger(2)} \tilde{\hat{P}}_\tau^{(2)} - \kappa_\tau : \hat{Q}_\tau \cdot \hat{Q}_\tau :, \tag{9}$$

where :: represents the normal ordering, and $c_{jm\tau}$ is either a neutron-hole annihilation operator ($\tau = \nu$) or a proton-particle annihilation operator ($\tau = \pi$). The monopole pair-creation

operator $\hat{P}^{\dagger(0)}_{\tau}$, the quadrupole pair-creation operator $\hat{P}^{\dagger(2)}_{M\tau}$, and the quadrupole operator $\hat{Q}_{M\tau}$ are defined by

$$\hat{P}^{\dagger(0)}_{\tau} = \sum_{j} \frac{\sqrt{2j+1}}{2} A^{\dagger(0)}_{0\tau}(jj), \tag{10}$$

$$\hat{P}^{\dagger(2)}_{M\tau} = \sum_{j_1 j_2} Q_{j_1 j_2} A^{\dagger(2)}_{M\tau}(j_1 j_2), \tag{11}$$

$$\tilde{\hat{P}}^{(2)}_{M\tau} = (-)^M \hat{P}^{(2)}_{-M\tau}, \tag{12}$$

$$\hat{Q}_{M\tau} = \sum_{j_1 j_2} Q_{j_1 j_2} \left[c^{\dagger}_{j_1\tau} \tilde{c}_{j_2\tau}\right]^{(2)}_{M}, \tag{13}$$

with

$$\tilde{c}_{jm\tau} = (-1)^{j-m} c_{j-m\tau}, \tag{14}$$

$$Q_{j_1 j_2} = -\frac{\langle j_1 \| r^2 Y^{(2)} \| j_2 \rangle}{\sqrt{5}}, \tag{15}$$

where $A^{\dagger(J)}_{M\tau}(j_1 j_2)$ stands for the nucleon pair-creation operator given by Eq. (3).

The interaction between neutrons and protons $\hat{H}_{\nu\pi}$ is taken as

$$\hat{H}_{\nu\pi} = -\kappa_{\nu\pi} \hat{Q}_{\nu} \cdot \hat{Q}_{\pi}. \tag{16}$$

Here the operator $\hat{Q}_{\tau}$ is the quadrupole operator defined by Eq. (13). In the present scheme, harmonic oscillator basis states with the oscillator parameter $b = \sqrt{\hbar/M\omega}$ are used as the single-particle basis states.

The Hamiltonian in Eq. (8) is diagonalized in terms of the many-body basis wave functions in Eq. (7) as

$$\hat{H}|I_i; i\rangle = E(I_i; i)|I_i; i\rangle, \tag{17}$$

where $|I_i; i\rangle$ is the normalized eigenvector for the ith state with spin I_i, and $E(I_i; i)$ is the eigenenergy for the state $|I_i; i\rangle$.

III. RESULTS FOR EVEN-EVEN NUCLEI

Since the valence neutron holes and proton particles occupy the $0g_{7/2}$, $1d_{5/2}$, $1d_{3/2}$, $0h_{11/2}$, and $2s_{1/2}$ orbitals in the mass $A \sim 130$ region, we take into account the full 50–82 configuration space for neutrons and protons.

The single-particle energies employed in the previous systematic calculations for the Xe, Ba, Ce, and Nd isotopes [28] were extracted from experimental excitation energies and were fixed constant for all the nuclei. The calculations reproduced well the energy levels for both the yrast and quasi-γ bands, and the intraband and interband $B(E2)$ values in the even-even isotopes. However, the theoretical results of the odd-mass isotopes were not satisfactory enough to describe the relative positions of the energy levels of positive-parity states and those of negative-parity states, especially for proton-odd nuclei. A similar situation was also seen in the results of the doubly odd nuclei [31], which were obtained by using constant single-particle energies. The doublet bands with the $\nu h_{11/2} \otimes \pi h_{11/2}$ configuration in theory were reproduced higher in energy than experimental ones. These results clearly indicate a need to shift the single-particle energy of the $0h_{11/2}$ orbital relative to the others. Thus, in the present study, we assume that the single-particle energies of some orbitals besides the $0h_{11/2}$ orbital change linearly with the number of valence particles.

The single-particle energies in the present analysis are determined by the following procedure. Since the small change of the single-particle energies hardly influences the energy levels of even-even nuclei, the single-particle energies are determined primarily to reproduce the energy levels of low-lying states for odd-mass nuclei. Using the same set of two-body interactions adopted in the previous PTSM studies [28], we first adjust the single-particle energies so as to approximately reproduce the energy levels of low-lying states for odd-mass nuclei. Next, the strengths of the two-body interactions are determined to reproduce the energy spectra of even-even nuclei. As shown later, the strengths of the two-body interactions change linearly with the number of valence particles. Finally, the single-particle energies are again modified to get an improved fitting, to the low-energy levels of odd-mass nuclei. The single-particle energies are thus obtained by repeating the above procedure, iteratively.

The determined functional dependences of the correction terms σ_{ν} and σ_{π} to the constant single-particle energies are as follows (in MeV):

$$\sigma_{\nu} = +0.02\bar{N}_{\nu} + 0.06N_{\pi} - 0.02, \tag{18}$$

$$\sigma_{\pi} = -0.02\bar{N}_{\nu} - 0.15N_{\pi} + 0.15, \tag{19}$$

where $\bar{N}_{\nu}$ indicates the number of valence neutron holes and N_{π}, the number of valence proton particles. The single-particle energies $\varepsilon_{j\tau}$ ($\tau = \nu$ or π) employed in the present calculations are listed in Table I. Note that the experimental excitation energies of ^{131}Sn are given when $\bar{N}_{\nu} = 1$ and $N_{\pi} = 0$, and those of ^{133}Sb are given when $\bar{N}_{\nu} = 0$ and $N_{\pi} = 1$.

In order to determine two-body interactions for even-even nuclei we use a χ^2 fitting as follows. Several sets of candidates for two-body interactions are searched to get smaller values of the following χ^2 values:

$$\chi^2 = \sum W(I; i)[E_{\text{expt}}(I; i) - E_{\text{th}}(I; i)]^2, \tag{20}$$

where $W(I; i)$ is a weight function for the ith state with spin I, $E_{\text{expt}}(I; i)$ represents the experimental energy, and $E_{\text{th}}(I; i)$, the theoretically predicted energy by the PTSM. As for the fitting energy levels, we take the low-lying states of the even-even isotopes, $^{128-132}$Xe, $^{130-134}$Ba, and $^{132-136}$Ce. We take $W(I; i) = 0$ for those levels that are not experimentally confirmed. The adopted values of weight functions are listed in Table II.

In order to investigate the systematics of low-lying states in the mass $A \sim 130$ region, we assume that the strengths of

TABLE I. Adopted single-particle energies $\varepsilon_{j\tau}$ ($\tau = \nu$ or π) for neutron holes or proton particles (in MeV). The numerals are extracted from experimental excitation energies in Refs. [37–39], and the correction terms σ_{ν} and σ_{π} are given in Eqs. (18) and (19), respectively.

j	$2s_{1/2}$	$0h_{11/2}$	$1d_{3/2}$	$1d_{5/2}$	$0g_{7/2}$
$\varepsilon_{j\nu}$	0.332	$0.242 + \sigma_{\nu}$	0.000	1.655	2.434
$\varepsilon_{j\pi}$	$2.990 + \sigma_{\pi}$	$2.793 + \sigma_{\pi}$	$2.708 + \sigma_{\pi}$	0.962	0.000

TABLE II. Adopted weight functions $W(I;i)$ for χ^2 fitting (in MeV^{-2}).

$\bar{N}_\nu + N_\pi$	2_1^+	4_1^+	6_1^+	2_2^+	3_1^+	4_2^+	5_1^+
8	1.00	1.00	0.16	1.00	0.64	0.25	0.09
10	1.00	1.00	0.64	1.00	0.64	0.25	0.09
12–20	1.00	1.00	1.00	1.00	0.64	0.25	0.09

the two-body interactions change linearly with the number of valence neutron holes $\bar{N}_\nu$ and valence proton particles N_π. The determined interaction strengths are as follows ($G_{0\tau}$ of MP interaction in units of MeV, and $G_{2\tau}$ of QP interaction and κ_τ of QQ interaction both in units of MeV/b^4):

$$\begin{aligned} G_{0\nu} &= 0.150 - 0.010\bar{N}_\nu - 0.002N_\pi, \\ G_{2\nu} &= 0.004 + 0.001\bar{N}_\nu + 0.002N_\pi, \\ \kappa_\nu &= 0.070 - 0.001\bar{N}_\nu + 0.001N_\pi, \\ G_{0\pi} &= 0.150 - 0.010\bar{N}_\nu, \\ G_{2\pi} &= 0.008 - 0.0005\bar{N}_\nu + 0.001N_\pi, \\ \kappa_\pi &= 0.020 + 0.002N_\pi, \\ \kappa_{\nu\pi} &= -0.060 - 0.001\bar{N}_\nu + 0.002N_\pi. \end{aligned} \tag{21}$$

This choice of the strengths of interactions gives the χ^2 value $\chi^2 = 0.705$ for 104 levels of even-even nuclei, $^{126-132}$Xe, $^{128-134}$Ba, $^{130-136}$Ce, and $^{132-138}$Nd.

A. Energy spectra

Using the interaction strengths determined above, the energy spectra are obtained for the even-even nuclei, $^{134-126}$Xe, $^{136-128}$Ba, $^{138-130}$Ce, and $^{140-132}$Nd. In Fig. 1, the theoretical energy spectra of the PTSM are compared with the experimental data for ^{132}Ba and ^{128}Xe. In both nuclei, the model reproduces well the energy levels of the even-spin yrast states up to spin 6. The level spacings between the yrast 8_1^+ and 10_1^+ states are small in experiment. The anomalous behavior at spin 10 is attributed to the alignment of two neutrons in the $0h_{11/2}$ orbital. For a description of them, we need to extend the SD version of the PTSM to include high-spin pairs coming from the $0h_{11/2}$ orbital [27,29]. We do not discuss those high-spin states in any further detail, since the focus of this paper is on the low-lying states. Concerning the quasi-γ bands, the energy staggering feature of the 3_1^+ and 4_2^+ states is reproduced in both nuclei, which indicates a triaxial nature of these nuclei.

In Fig. 2, the energy spectra obtained by the PTSM are compared with the experimental data for even-even Xe isotopes. For ^{132,130,126}Xe, the energy levels of the even-spin yrast states are well reproduced. The staggering patterns of the energy levels in the quasi-γ bands are also described well, indicating the γ instability in the low-lying states. We have not used the experimental information on the 0_2^+ states for the χ^2 fitting, but the theoretical 0_2^+ state comes close to the corresponding experimental one in each nucleus. Concerning ^{134}Xe, the theoretical energy level of the 4_1^+ state is a bit lower, and those of the 5_1^+ and 6_1^+ states are a bit higher in energy than the experimental ones. For an $N = 80$ nucleus

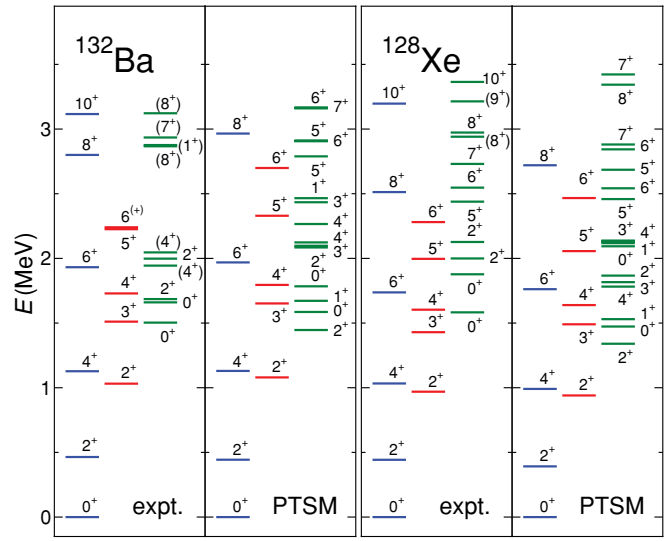

FIG. 1. (Color online) Comparison between the experimental energy spectra (expt.) and those of the PTSM (PTSM) for ^{132}Ba and ^{128}Xe. The level sequences on the left represent the yrast band, and the level sequences on the middle, the quasi-γ band. The experimental data are taken from Refs. [40–46].

near a single closed shell like ^{134}Xe, higher-spin collective pairs play important roles because the quadrupole collectivity is not dominant near the closed shell.

In Fig. 3, the theoretical energy levels of the low-lying states are compared with the experimental data for ^{136,134,130,128}Ba. Except for ^{136}Ba, the PTSM calculations are in better agreement with the experimental data than those of the Xe isotopes. This means that the quadrupole collectivity becomes more dominant in the low-lying states of the Ba isotopes, which have two more valence protons. The experimental energy staggering for the even-odd spin states in the quasi-γ band is well reproduced. As in ^{134}Xe, in ^{136}Ba, higher-spin pairs play important roles to describe the 6_1^+ state, which is very close to the 4_1^+ state in experiment.

Figures 4 and 5 show the theoretical spectra of even-even Ce and Nd isotopes, respectively, compared with the experimental data. One sees that there is a good correspondence between the theoretical and experimental levels and the ordering of the 2_2^+ and 0_2^+ states is reproduced except for ^{138}Ce near the single closed shell.

In Figs. 1–5 we notice that theoretical excitation energies for the yrast and quasi-γ bands smoothly decrease as the number of neutron holes increases, which accords with the experimental tendency. Also the staggering patterns of the energy levels in the quasi-γ bands are well reproduced.

The systematic calculations in the even-even and odd-mass nuclei in this mass region were performed in terms of the SD version of the PTSM [28]. The experimental energy levels of the yrast and quasi-γ bands for Xe, Ba, Ce, and Nd isotopes were well reproduced except for the $N = 72$ isotones, where the calculated energy levels for the quasi-γ band were lower in energy than the experimental ones. The results of the present calculations on energy levels are improved and are generally

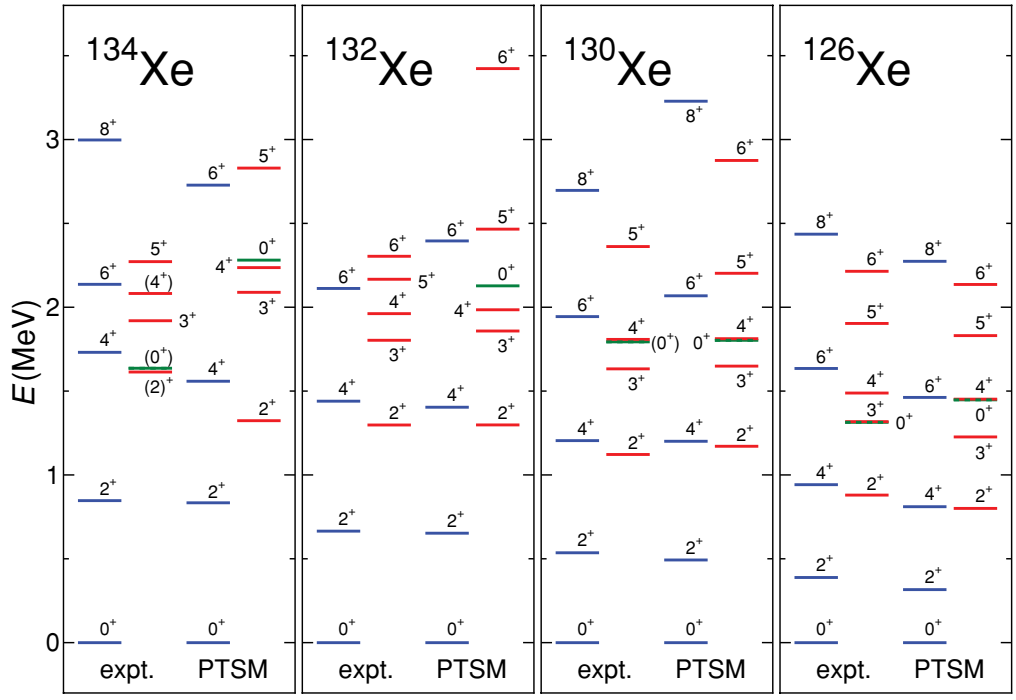

FIG. 2. (Color online) Comparison between the experimental energy spectra (expt.) and those of the PTSM (PTSM) for ^{134,132,130,126}Xe. The level sequences on the left represent the yrast band, and the level sequences on the right, the 2_2^+, 3_1^+, 4_2^+, 5_1^+, 6_2^+, and 0_2^+ states. The experimental data are taken from Refs. [40,47–51].

in better agreement with the experimental data than those of the previous PTSM study [28]. For example, the description of the excitation energies for the 3_1^+ and 5_1^+ states in ^{126}Xe and ^{128}Ba is much improved.

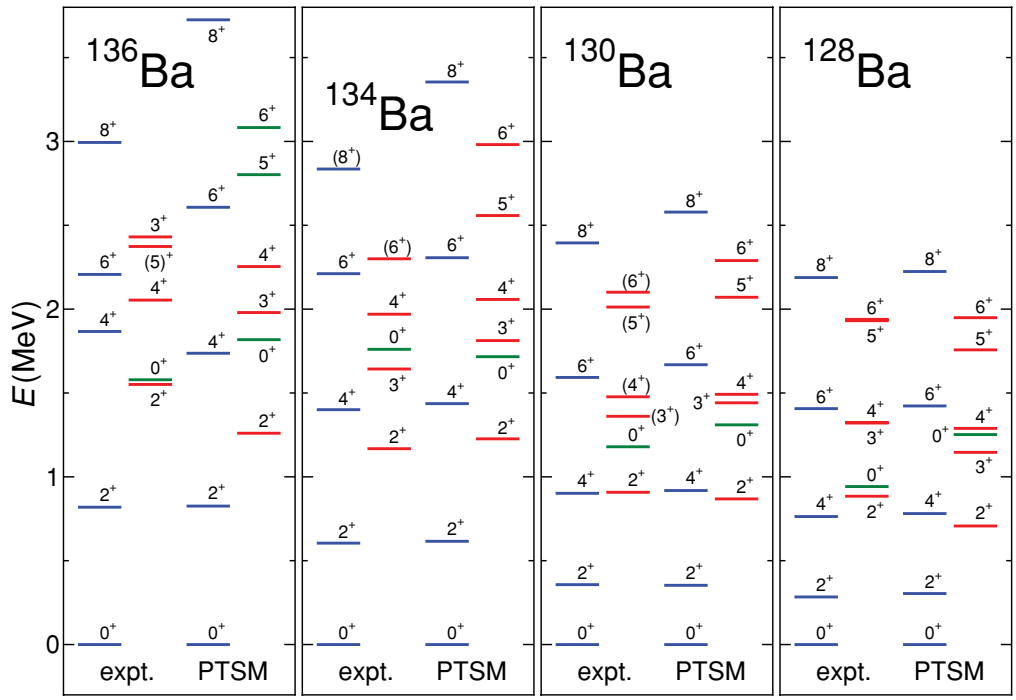

FIG. 3. (Color online) Same as Fig. 2, but for ^{136,134,130,128}Ba. The experimental data are taken from Refs. [52–59].

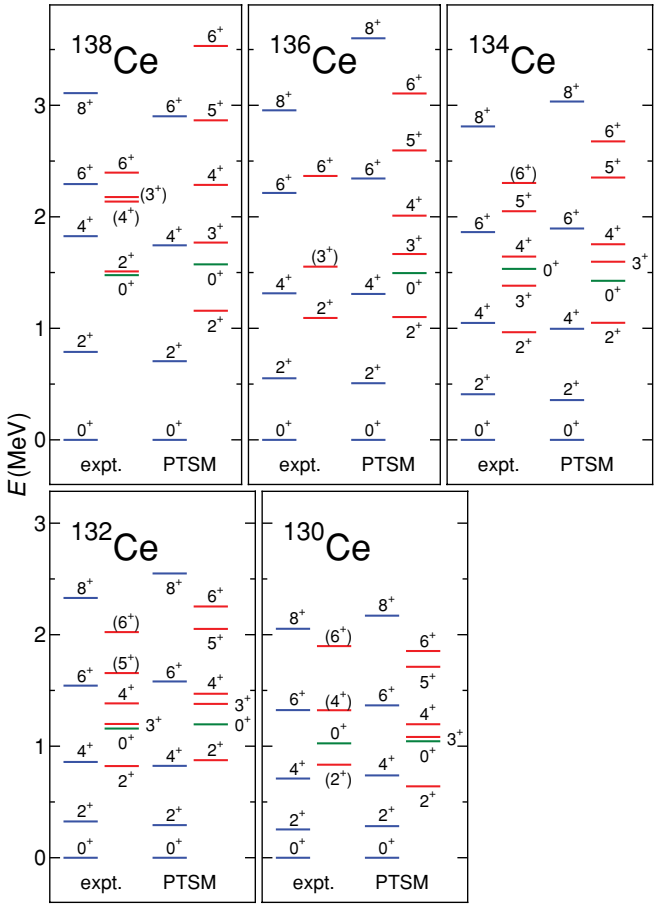

FIG. 4. (Color online) Same as Fig. 2, but for ^{138,136,134,132,130}Ce. The experimental data are taken from Refs. [60–66].

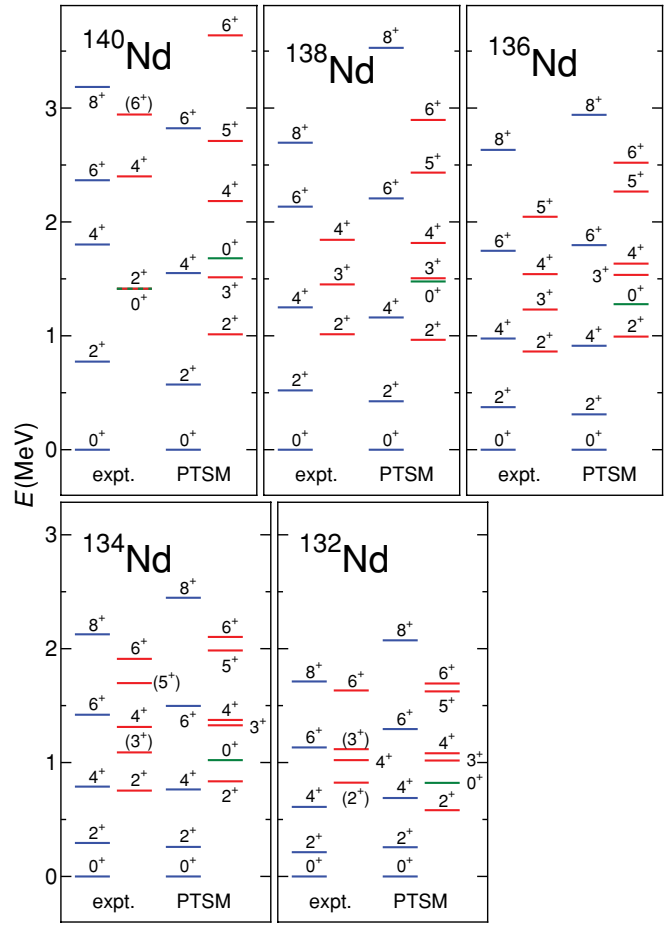

FIG. 5. (Color online) Same as Fig. 2, but for ^{140,138,136,134,132}Nd. The experimental data are taken from Refs. [67–73].

B. $E2$ transition rates

The $E2$ transition rate is calculated as

$$B(E2, I_i \to I_f) = \frac{1}{2I_i + 1} |\langle I_f; f \| \hat{T}(E2) \| I_i; i \rangle|^2, \quad (22)$$

where $|I_i; i\rangle$ represents the wave function for the ith state with spin I_i obtained by diagonalizing the shell-model Hamiltonian in Eq. (8). Here, the $E2$ transition operator is defined as

$$\hat{T}(E2; M) = e_\nu \hat{Q}_{M\nu} + e_\pi \hat{Q}_{M\pi}, \quad (23)$$

where e_τ ($\tau = \nu$ or π) represents the effective charge of the nucleon, and the operator $\hat{Q}_\tau$ is the quadrupole operator defined by Eq. (13) with the oscillator parameter $b = 1.005A^{1/6}$ fm. The effective charges are assumed to follow the conventional relation $e_\nu = -\delta e$ and $e_\pi = (1 + \delta)e$ [74], and the adopted values are $\delta = 0.96 + 0.04\bar{N}_\nu - 0.03N_\pi$. They are fixed so as to reproduce the experimental $B(E2; 2_1^+ \to 0_1^+)$ values of the even-even nuclei. Note that the neutron effective charge is chosen to be negative, as valence neutrons are treated as holes.

In Fig. 6 the calculated $B(E2; 2_1^+ \to 0_1^+)$ values are compared with the experimental data for even-even Xe, Ba, Ce, and Nd isotopes. The theoretical results are in good agreement with the experimental data, except for the transition of ^{132}Nd. This discrepancy may suggest that the deformation obtained by the SD truncation scheme is smaller than the experimental one.

Table III shows calculated relative $B(E2)$ values between low-lying states for even-even Ba and Xe isotopes in comparison with the experimental data, and also with the O(6) limit of the IBM. It is seen that in ^{132,130,128}Ba and ^{128,126}Xe, the theoretical results reproduce very well the experimental data and simulate the results in the O(6) limit of the IBM, which is known to describe γ-unstable nuclei. In the case of ^{134}Ba, the theoretical $E2$ transition of $0_2^+ \to 2_1^+$ is much larger and that of $4_2^+ \to 4_1^+$ is a bit smaller in our calculation than the experimental data, but the other transitions are in satisfactory agreement. The large $0_2^+ \to 2_1^+$ transition rate might come from the different level ordering of 0_2^+ and 0_3^+, since we can obtain the small ratio $B(E2; 0_3^+ \to 2_1^+)/B(E2; 0_3^+ \to 2_2^+) = 0.000\,52$ for ^{134}Ba. The large disagreements between the experimental and calculated $E2$ transitions of $0_2^+ \to 2_1^+$ and $4_2^+ \to 4_1^+$ are similar to those obtained by the previous study [28].

In Table IV, the theoretical relative $B(E2)$ values in low-lying states are compared with the experimental data for Ce isotopes. In ^{134}Ce and ^{132}Ce, good agreement between theoretical relative $B(E2)$ values and the experimental data is achieved. In particular, small $E2$ interband transitions such as the $3_1^+ \to 2_1^+$ and $4_2^+ \to 2_1^+$ transitions are well reproduced. Note that no experimental data are available for ^{136}Ce and ^{130}Ce. The PTSM results of both nuclei predict the properties very close to the O(6) limit.

TABLE III. Comparison of calculated relative $B(E2)$ values (PTSM) for ^{134,132,130,128}Ba and ^{128,126}Xe, the experimental data (Expt.), and the prediction of the O(6) limit of the IBM [O(6)]. The experimental data are taken from Refs. [44,46,51,55,57,76].

$I_i^\pi \to I'^\pi_f$	^{134}Ba		^{132}Ba		^{130}Ba		^{128}Ba		^{128}Xe		^{126}Xe		O(6)
	PTSM	Expt.	PTSM	Expt.	PTSM	Expt.	PTSM	Expt.	PTSM	Expt.	PTSM	Expt.	
$2_2^+ \to 2_1^+$	100	100	100	100	100	100	100	100	100	100	100	100	100
$\to 0_1^+$	0.24	0.9(2)	1.1	2.7(4)	0.72	6.2(7)	1.1	11.7(10)	0.093	1.3^{+5}_{-3}	2.3	1.5(2)	0
$3_1^+ \to 2_2^+$	100	100	100	100	100	100	100	100	100	100	100	100	100
$\to 4_1^+$	15	$\geqslant$2.6	16	38(6)	27	22(3)	37	16.5(25)	29	35^{+15}_{-11}	34	32(5)	40
$\to 2_1^+$	2.3	1.1	0.98	2.6(4)	0.16	4.5(6)	4.4	6.3(13)	2.5	1.6^{+7}_{-5}	6.5	1.8(3)	0
$4_2^+ \to 2_2^+$	100	100	100	100	100	100	100	100	100	100	100	100	100
$\to 3_1^+$	25		12	$\leqslant$50(11)	0.68		0.13		0.98		12		0
$\to 4_1^+$	25	73	48	73(10)	67	54(10)	93	27.6(52)	88	102^{+23}_{-19}	88	74^{+12}_{-13}	91
$\to 2_1^+$	19	2.4	3.4	1.8(3)	0.39	2.3(4)	0.041	1.9(3)	0.11	1.8^{+4}_{-3}	0.071	0.42(7)	0
$5_1^+ \to 3_1^+$	100	100	100	100	100	100	100	100	100	100	100	100	100
$\to 4_2^+$	67		39	$\leqslant$45(7)	38		48		0.51		42	73(14)	46
$\to 6_1^+$	12		7.5		19		35		0.87		19	95(48)	45
$\to 4_1^+$	0.35		0.095	$\leqslant$2.2(3)	0.69		4.2		0.25		3.5	1.1(5)	0
$0_2^+ \to 2_2^+$	100	100	100	100	100	100	100	100	100	100	100	100	100
$\to 2_1^+$	119	3.5	3.3	$\leqslant$0.7(1)	0.71	3.3(2)	0.022		$<$0.01	7.0^{+25}_{-18}	0.78	9.1(1)	0

C. $M1$ transition rates

The $M1$ transition rate is calculated as

$$B(M1, I_i \to I_f) = \frac{1}{2I_i + 1} |\langle I_f; f \| \hat{T}(M1) \| I_i; i \rangle|^2, \quad (24)$$

where $|I_i; i\rangle$ represents the wave function for the ith state with spin I_i obtained by diagonalizing the shell-model Hamiltonian in Eq. (8). Here, the $M1$ transition operator is defined as

$$\hat{T}(M1; M) = \mu_N \sqrt{\frac{3}{4\pi}} \sum_{\tau=\nu,\pi} [g_{\ell\tau} \hat{\boldsymbol{j}}_\tau + (g_{s\tau} - g_{\ell\tau}) \hat{\boldsymbol{s}}_\tau]_M, \quad (25)$$

where μ_N ($=e\hbar/2mc$) is the nuclear magneton, and $g_{\ell\nu}$ ($g_{s\nu}$) and $g_{\ell\pi}$ ($g_{s\pi}$) represent the gyromagnetic ratios for orbital angular momentum (spin) for the neutron and the proton, respectively. The operators $\hat{\boldsymbol{j}}$ and $\hat{\boldsymbol{s}}$ stand for the angular momentum and spin operators, respectively. The adopted gyromagnetic ratios for orbital angular momenta are $g_{\ell\nu} = 0.00$, $g_{\ell\pi} = 1.00$, and those for spin are $g_{s\nu} = -2.68$ and $g_{s\pi} = 3.91$, which are free-nucleon g factors attenuated by a factor of 0.7.

In Table V, we show the calculated excitation energies of the 1_i^+ states ($i = 1,2,3,4$), and the $B(M1)$ values (in $10^{-2}\mu_N^2$) from the ground states (the $0^+_{\text{g.s.}}$ states) to the 1_i^+ states for Ba and Ce isotopes. It is seen that for each nucleus the $B(M1)$ strength from the ground state is concentrated in the lowest 1^+ (1_1^+) state. The $B(M1; 0^+_{\text{g.s.}} \to 1_i^+)$ values for ^{132}Ba were previously calculated by the $SD + H$ version of the PTSM [27]. In the previous calculation the transition to the

TABLE IV. Comparison of calculated relative $B(E2)$ values (PTSM) for ^{136,134,132,130}Ce, and the experimental data (Expt.). The experimental data are taken from Refs. [65,66]. No experimental data are available for ^{136,130}Ce.

$I_i^\pi \to I'^\pi_f$	^{136}Ce	^{134}Ce		^{132}Ce		^{130}Ce
	PTSM	PTSM	Expt.	PTSM	Expt.	PTSM
$2_2^+ \to 2_1^+$	100	100	100	100	100	100
$\to 0_1^+$	0.016	3.5	5.4	3.5	6.1	0.20
$3_1^+ \to 2_2^+$	100	100	100	100	100	100
$\to 4_1^+$	21	17	25.0	22	29.1(7)	37
$\to 2_1^+$	1.8	0.064	2.2	0.64	4.0	1.5
$4_2^+ \to 2_2^+$	100	100	100	100	100	100
$\to 3_1^+$	29	27		23		0.83
$\to 4_1^+$	47	39	55.0	44	59	91
$\to 2_1^+$	0.38	0.091	0.63	$<$0.01	0.42	0.64
$5_1^+ \to 3_1^+$	100	100	100	100	100	100
$\to 4_2^+$	54	45		46		48
$\to 6_1^+$	20	15		22		39
$\to 4_1^+$	1.3	0.29	$\leqslant$5.6	0.21		3.6
$0_2^+ \to 2_2^+$	100	100	100	100	100	100
$\to 2_1^+$	26	3.8	$\leqslant$2.7	2.2	0.56	0.30

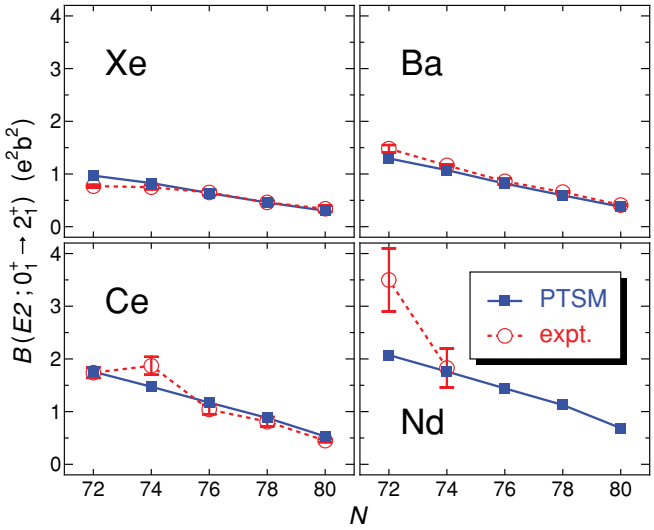

FIG. 6. (Color online) Comparison of the calculated $B(E2)$ values from the ground state to the first 2^+ state for Xe, Ba, Ce, and Nd isotopes with the experimental data. The experimental data are taken from Ref. [75].

1_1^+ state (1.941 MeV) was strongest [$B(M1;0_{\text{g.s.}}^+ \rightarrow 1_1^+) = 0.595\mu_N^2$] among all the transitions. In the present calculation the energy of the 1_1^+ state (1.672 MeV) is predicted to be a bit lower than that of the previous calculation. Since the model space in the present study is smaller than that in the previous study (the truncated $SD + H$ space), we may underestimate the excitation energy of the 1_1^+ state. Thus it might not be appropriate to discuss further the detailed results of magnetic excitation states because the present scheme only uses the collective S and D pairs

Table VI shows the theoretical excitation energies of the 2_i^+ states ($i = 2, 3, 4, 5$), and $B(M1;2_i^+ \rightarrow 2_1^+)$ values for Ba and Ce isotopes. For each nucleus the $M1$ transition from the 2_3^+ state at around 1.5 MeV is the largest among all the transitions, showing that they are candidates for the mixed-symmetry states [46,77,78].

D. Magnetic and quadrupole moments

The magnetic dipole moment is calculated as

$$\mu(I_i) = \langle I_i I_i; i | \hat{\boldsymbol{\mu}}_{m=0} | I_i I_i; i \rangle, \tag{26}$$

where $|IM;i\rangle$ represents the wave function for the ith state with spin I and its projection M. The magnetic dipole operator is written as

$$\hat{\boldsymbol{\mu}} = \mu_N \sum_{\tau=\nu,\pi} [g_{\ell\tau} \hat{\boldsymbol{j}}_\tau + (g_{s\tau} - g_{\ell\tau}) \hat{\boldsymbol{s}}_\tau], \tag{27}$$

where the operators $\hat{\boldsymbol{j}}$ and $\hat{\boldsymbol{s}}$, and the gyromagnetic ratios are taken to be the same as used for the $M1$ transition rates.

The electric quadrupole moment is calculated as

$$Q(I_i) = \langle I_i I_i; i | \hat{Q}_0 | I_i I_i; i \rangle. \tag{28}$$

Here, the electric quadrupole operator is given by

$$\hat{Q}_M = \sqrt{\frac{16\pi}{5}} (e_\nu \hat{Q}_{M\nu} + e_\pi \hat{Q}_{M\pi}), \tag{29}$$

where e_τ ($\tau = \nu$ or π) represents the effective charge of the nucleon. The quadrupole operator $\hat{Q}_\tau$, the effective charges, and the oscillator parameter are taken to be the same as used for the $E2$ transition rates.

In Table VII, the calculated magnetic and quadrupole moments for even-even Xe and Ba isotopes are compared with the experimental data. The calculated magnetic moments of the 2_1^+ states decrease as a function of the number of neutron holes. Our calculations reproduce well the experimental magnetic moments except for the 2_1^+ states of ^{128}Xe, ^{126}Xe, and ^{130}Ba, which have neutron holes more than or equal to 8. This might be due to the fact that single-particle levels with positive parity are easily admixed by quadrupole deformation which is expected to be large in eight-neutron-hole systems.

For the quadrupole moments, there are only a few experimental data. The undecided candidates for the quadrupole moments of the 2_1^+ states are reported for ^{136}Ba, ^{134}Ba, and ^{130}Ba. Our results suggest the quadrupole moments of +0.07(7), −0.13(16), and −0.1(2) for ^{136}Ba, ^{134}Ba, and ^{130}Ba, respectively.

In Table VIII, the theoretical magnetic and quadrupole moments of the PTSM are compared with the experimental data for even-even Ce and Nd isotopes. Unfortunately, the magnetic moment of the 2_1^+ state only for ^{134}Nd is available. This moment is well reproduced by the PTSM within the experimental error.

IV. RESULTS FOR ODD-MASS NUCLEI

In order to describe odd-mass nuclei, we need to expand the model space to include an unpaired nucleon in addition to the SD-pair state [26,28]. If the nucleon creation operator $c_{jm}^\dagger$ (neutron-hole creation operator or proton-particle creation operator) is applied to the SD-pair state, the odd-nucleon state,

TABLE V. Calculated excitation energies of the 1_i^+ states (in MeV), and $B(M1;0_{\text{g.s.}}^+ \rightarrow 1_i^+)$ values (in $10^{-2}\mu_N^2$) for Ba and Ce isotopes.

i	^{134}Ba		^{132}Ba		^{130}Ba		^{136}Ce		^{134}Ce		^{132}Ce	
	Energy	$B(M1)$	Energy	$B(M1)$	Energy	$B(M1)$	Energy	$B(M1)$	Energy	$B(M1)$	Energy	$B(M1)$
1	1.921	21.0	1.672	39.3	1.586	59.3	1.855	41.8	1.684	73.2	1.651	102.6
2	2.744	2.34	2.466	6.01	2.241	8.82	2.572	4.95	2.515	7.94	2.358	9.75
3	3.088	3.35	2.875	4.53	2.640	4.33	2.992	1.77	2.979	1.42	2.802	0.926
4	3.730	0.151	3.376	0.136	3.091	0.459	3.609	< 0.1	3.399	0.279	3.153	0.386

TABLE VI. Calculated excitation energies of the 2_i^+ states (in MeV) and $B(M1; 2_i^+ \to 2_1^+)$ values (in $10^{-2}\mu_N^2$) for ^{134,132,130}Ba and ^{136,134,132}Ce.

i	^{134}Ba		^{132}Ba		^{130}Ba		^{136}Ce		^{134}Ce		^{132}Ce	
	Energy	$B(M1)$	Energy	$B(M1)$	Energy	$B(M1)$	Energy	$B(M1)$	Energy	$B(M1)$	Energy	$B(M1)$
2	1.227	15.6	1.080	5.98	0.898	3.75	1.101	12.2	1.050	4.91	0.875	3.69
3	1.619	16.1	1.446	22.0	1.448	27.3	1.588	18.0	1.588	32.1	1.563	29.9
4	2.189	9.04	2.085	5.50	1.914	8.85	2.090	2.61	2.051	0.121	1.867	25.5
5	2.365	4.63	2.158	0.658	2.000	1.79	2.212	6.57	2.095	8.48	2.020	<0.1

i.e., the SD pairs plus one-particle state, is constructed as

$$|jS^{n_s}D^{n_d}(I\eta)\rangle = [c_j^\dagger |S^{n_s}D^{n_d}(I'\eta)\rangle]^{(I)}, \quad (30)$$

where I' is the total angular momentum of the SD pair state, I is the total angular momentum of the SD pair plus one-particle state, and η is an additional quantum number required to completely specify the state. Due to this extension, the PTSM can treat even-even, odd-mass, and doubly odd nuclei on the same footing. Using the SD pair plus one-particle state in neutron space and the SD-pair state in proton space in Eq. (6), we can express the many-body wave function of the odd-even (neutron-odd and proton-even) nucleus with spin I and its projection M as

$$|\Phi(IM\eta)\rangle = [|j_\nu S^{\bar{n}_s}D^{\bar{n}_d}(I_\nu\eta_\nu)\rangle \otimes |S^{n_s}D^{n_d}(I_\pi\eta_\pi)\rangle]^{(I)}_M, \quad (31)$$

where $2(\bar{n}_s + \bar{n}_d) + 1$ and $2(n_s + n_d)$ are the total number of valence neutron holes $\bar{N}_\nu$ and that of valence proton particles N_π, respectively. For even-odd (neutron-even and proton-odd) nuclei, the many-body wave function can be written as

$$|\Phi(IM\eta)\rangle = [|S^{\bar{n}_s}D^{\bar{n}_d}(I_\nu\eta_\nu)\rangle \otimes |j_\pi S^{n_s}D^{n_d}(I_\pi\eta_\pi)\rangle]^{(I)}_M. \quad (32)$$

Here, $\bar{N}_\nu = 2(\bar{n}_s + \bar{n}_d)$, and $N_\pi = 2(n_s + n_d) + 1$. As for the single-particle energies and the two-body interaction strengths, we use the same set of interactions as used in the even-even nuclei.

A. Energy spectra

Figure 7 shows the comparison of the calculated energy spectra obtained by the PTSM (at most up to the second level for each spin I) with the experimental data for odd-mass Xe isotopes. In experiment, the level spacing between the ground state ($3/2_1^+$) and the first excited state ($1/2_1^+$) decreases smoothly as a function of the number of neutron holes, and the ordering of these states changes in ^{129}Xe. Our calculation successfully reproduces this behavior except for the $N = 79$

TABLE VII. Comparison of the magnetic dipole moments μ (in μ_N) and electric quadrupole moments Q (in eb) obtained by the PTSM (PTSM) with the experiment data (Expt.) for even-even Xe and Ba isotopes. The experimental data are taken from Ref. [79].

Nucleus	I_i^π	μ		Q		Nucleus	I_i^π	μ		Q
		PTSM	Expt.	PTSM	Expt.			PTSM	Expt.	PTSM
^{134}Xe	2_1^+	+1.03	+0.708(14)	+0.0536		^{132}Xe	2_1^+	+0.743	+0.63(2)	−0.00626
	4_1^+	+2.64	+3.2(6)	+0.275			4_1^+	+2.19	+2.4(4)	+0.231
	6_1^+	+2.80		+0.400			6_1^+	+2.49		+0.288
	2_2^+	+0.462		+0.139			2_2^+	+0.540	+0.2(4)	−0.00831
^{130}Xe	2_1^+	+0.498	+0.67(2)	−0.109		^{128}Xe	2_1^+	+0.337	+0.82(14)	−0.0814
	4_1^+	+1.42	+1.7(2)	+0.0455			4_1^+	+0.879		+0.0135
	6_1^+	+2.12		+0.197			6_1^+	+1.51		+0.151
	2_2^+	+0.425	+0.9(2)	+0.252			2_2^+	+0.283		+0.106
^{136}Ba	2_1^+	+0.760	+0.69(10)	+0.0804	−0.19(6) or +0.07(7)	^{126}Xe	2_1^+	+0.160	+0.74(14)	+0.308
	4_1^+	+2.63		−0.184			4_1^+	+0.524		+0.278
	6_1^+	+4.06		+0.00220			6_1^+	+0.957		+0.292
	2_2^+	+0.838		−0.0438			2_2^+	+0.401		−0.262
^{134}Ba	2_1^+	+0.659	+0.86(10)	−0.124	−0.34(16) or −0.13(16)	^{132}Ba	2_1^+	+0.564	+0.68(6)	−0.341
	4_1^+	+2.02		−0.280			4_1^+	+1.50		−0.432
	6_1^+	+3.27		−0.191			6_1^+	+2.58		−0.414
	2_2^+	+0.694		+0.00677			2_2^+	+0.428		+0.313
^{130}Ba	2_1^+	+0.332	+0.70(6)	−0.365	−1.0(2) or −0.1(2)	^{128}Ba	2_1^+	+0.322		+0.124
	4_1^+	+1.15		−0.427			4_1^+	+0.793		+0.143
	6_1^+	+1.92		−0.452			6_1^+	+1.34		−0.0740
	2_2^+	+0.325		+0.371			2_2^+	+0.520		−0.0985

TABLE VIII. The same for even-even Ce and Nd isotopes as in Table VII. The experimental data are taken from Ref. [79].

Nucleus	I_i^π	μ	Q	Nucleus	I_i^π	μ	Q	Nucleus	I_i^π	μ		Q
		PTSM	PTSM			PTSM	PTSM			PTSM	Expt.	PTSM
^{138}Ce	2_1^+	+0.801	+0.102	^{136}Ce	2_1^+	+0.907	−0.367	^{134}Ce	2_1^+	+0.878		−0.728
	4_1^+	+2.56	−0.316		4_1^+	+2.14	−0.554		4_1^+	+1.88		−0.838
	6_1^+	+4.13	−0.411		6_1^+	+3.45	−0.611		6_1^+	+2.92		−0.829
	2_2^+	+1.11	−0.137		2_2^+	+0.651	+0.270		2_2^+	+0.397		+0.675
^{132}Ce	2_1^+	+0.797	−0.821	^{130}Ce	2_1^+	+0.597	−0.219	^{140}Nd	2_1^+	+0.873		+0.161
	4_1^+	+1.61	−0.904		4_1^+	+1.22	−0.256		4_1^+	+2.53		−0.274
	6_1^+	+2.41	−0.864		6_1^+	+1.86	−0.238		6_1^+	+4.26		−0.522
	2_2^+	+0.327	−0.113		2_2^+	+0.561	+0.220		2_2^+	+1.26		−0.152
^{138}Nd	2_1^+	+1.04	−0.488	^{136}Nd	2_1^+	+1.01	−0.888	^{134}Nd	2_1^+	+0.915	+1.2(4)	−0.987
	4_1^+	+2.26	−0.626		4_1^+	+2.09	−0.993		4_1^+	+1.83		−1.08
	6_1^+	+3.57	−0.671		6_1^+	+3.18	−0.944		6_1^+	+2.71		−1.01
	2_2^+	+0.690	+0.446		2_2^+	+0.447	+0.845		2_2^+	+0.362		+0.951
^{132}Nd	2_1^+	+0.742	−0.497									
	4_1^+	+1.45	−0.484									
	6_1^+	+2.14	−0.356									
	2_2^+	+0.532	+0.484									

nucleus, ^{131}Xe. In this nucleus, the level ordering of the $3/2_1^+$ and $1/2_1^+$ states is predicted in reverse, though these two states are almost degenerate in theory. Concerning other positive-parity states, the level orderings of the $5/2_1^+$ and $3/2_2^+$ states are predicted in reverse for ^{133}Xe and ^{131}Xe. However, for all the Xe isotopes, there exists a one-to-one correspondence between the theoretical and experimental levels for the $5/2_1^+$, $7/2_1^+$, and $3/2_2^+$ states.

Concerning the negative-parity states, the excitation energies of the $11/2_1^-$ states are in excellent agreement with the observation for ^{135,131,129}Xe. In the $N = 75$ nucleus, ^{129}Xe, the experimental $9/2_1^-$ state lies higher in energy than the $11/2_1^-$ state. The calculated $9/2_1^-$ state is a bit lower in energy than the $11/2_1^-$ state, but the result is within a reasonable range. In ^{133}Xe, the experimental $11/2_1^-$ state is higher in energy than the ground state $(3/2_1^+)$ while the PTSM predicts the $11/2_1^-$

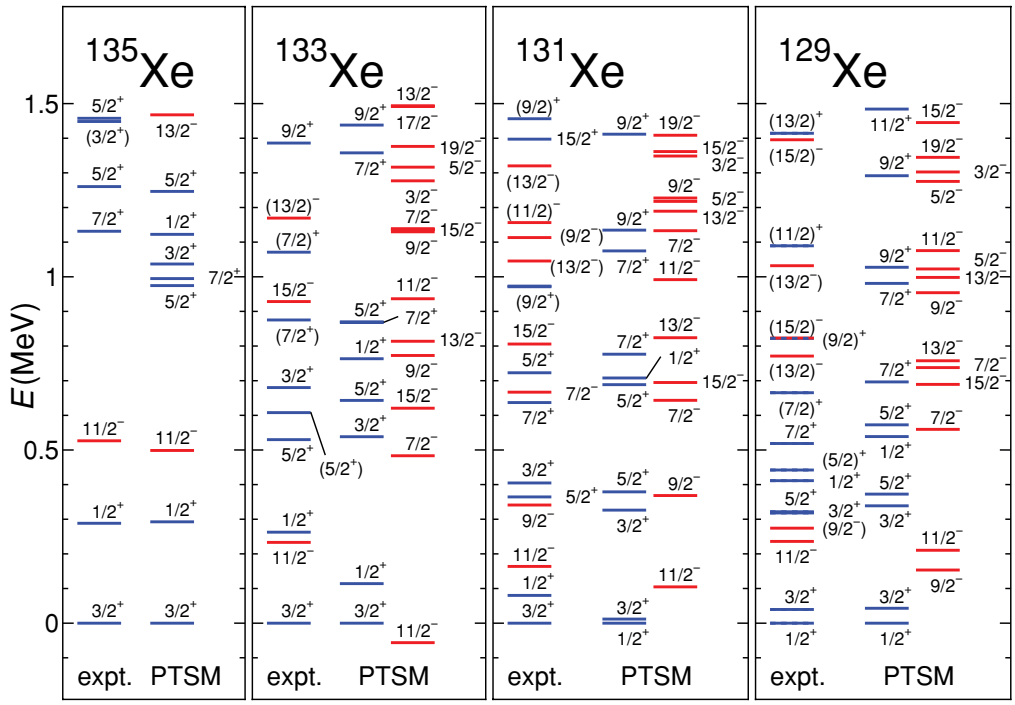

FIG. 7. (Color online) Comparison of the experimental energy levels (expt.) with those of theory (PTSM) for ^{135,133,131,129}Xe. The experimental data are taken from Refs. [80–84].

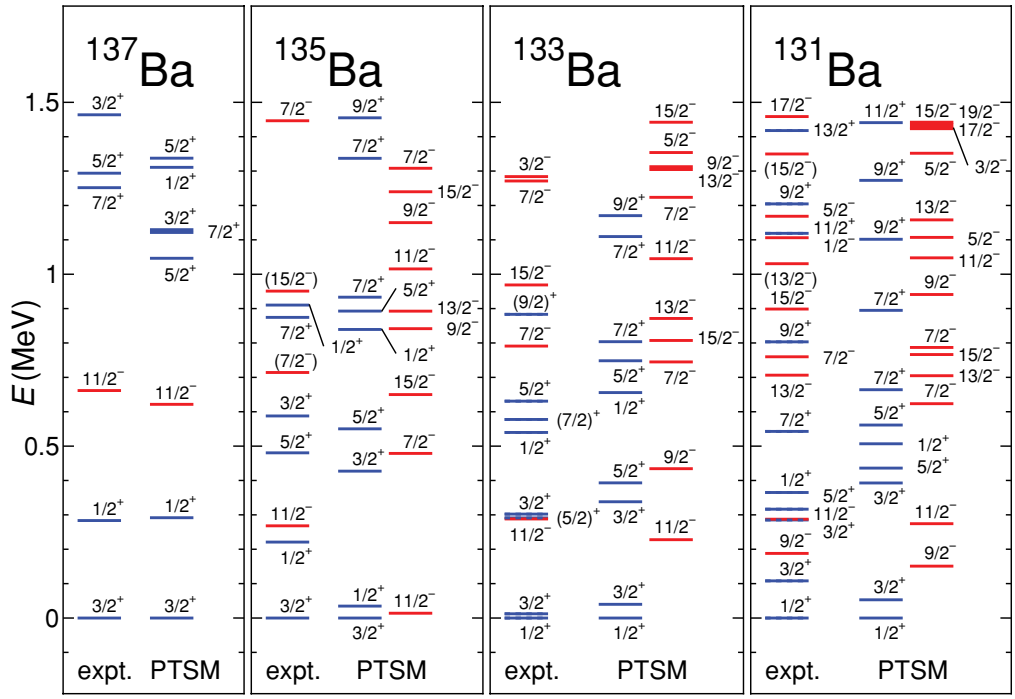

FIG. 8. (Color online) Same as Fig. 7, but for ^{137,135,133,131}Ba. The experimental data are taken from Refs. [81,83–88].

state to be the ground state. For reproduction of the ordering and position of this negative-parity state we may need higher-angular-momentum pairs such as angular-momentum-four (G) collective pairs, which are missing in the present scheme.

In Fig. 8, the theoretical energy spectra are compared with the experimental data for odd-mass Ba isotopes. As for the Xe isotopes, our calculation successfully reproduces the mild change of the ordering of $3/2^+_1$ and $1/2^+_1$ states between the four Ba isotopes. The theoretical energy levels of the $5/2^+_1$, $7/2^+_1$, and $3/2^+_2$ states are in good agreement with the experimental data. For the $N = 79$ nucleus, ^{135}Ba, the calculated $11/2^-_1$ state lies a bit lower in energy than the

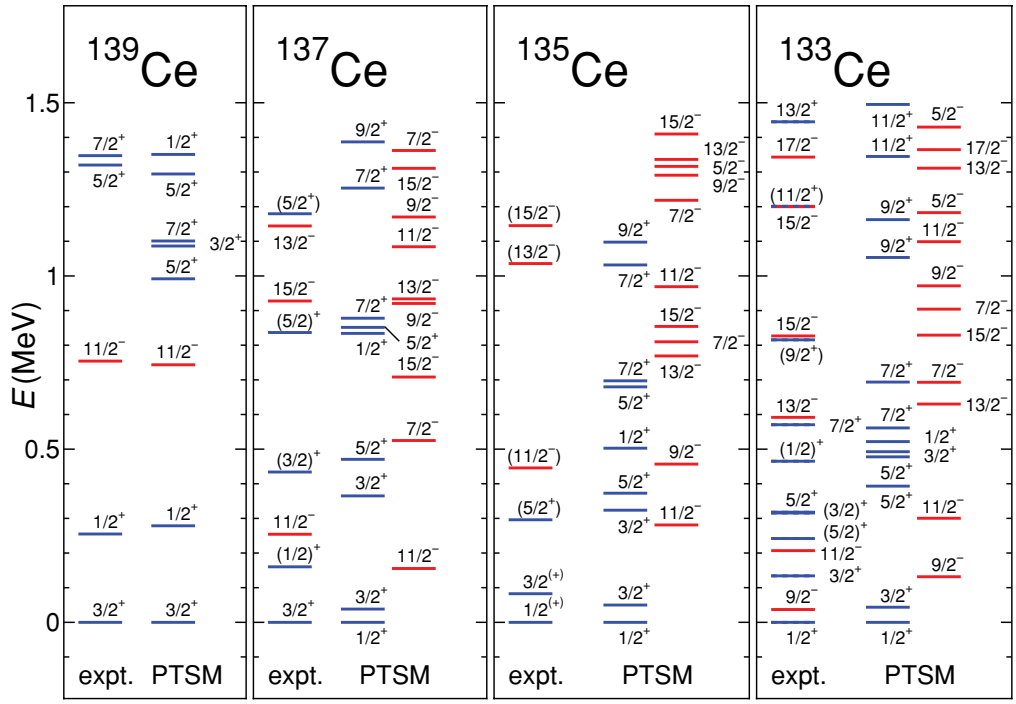

FIG. 9. (Color online) Same as Fig. 7, but for ^{139,137,135,133}Ce. The experimental data are taken from Refs. [81,84,86,89].

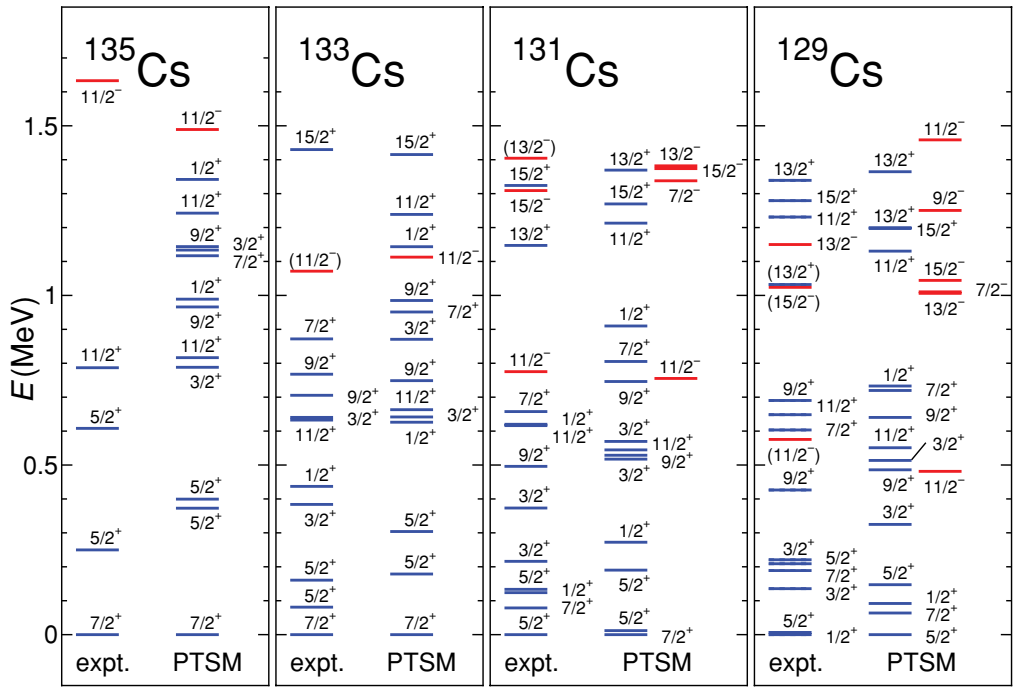

FIG. 10. (Color online) Same as Fig. 7, but for ^{135,133,131,129}Cs. The experimental data are taken from Refs. [81–84,90,91].

experimental one. In contrast to ^{129}Xe ($N = 75$ nucleus), in ^{131}Ba (also $N = 75$ nucleus) the PTSM calculation reproduces quite well the correct ordering of the $9/2^-_1$ and $11/2^-_1$ states.

The energy spectra for odd-mass Ce isotopes are shown in Fig. 9. In ^{137}Ce, our calculation seems to fail in predicting the experimental energy level of the $5/2^+_1$ state at the correct position, but the PTSM predicts another $5/2^+$ state at around

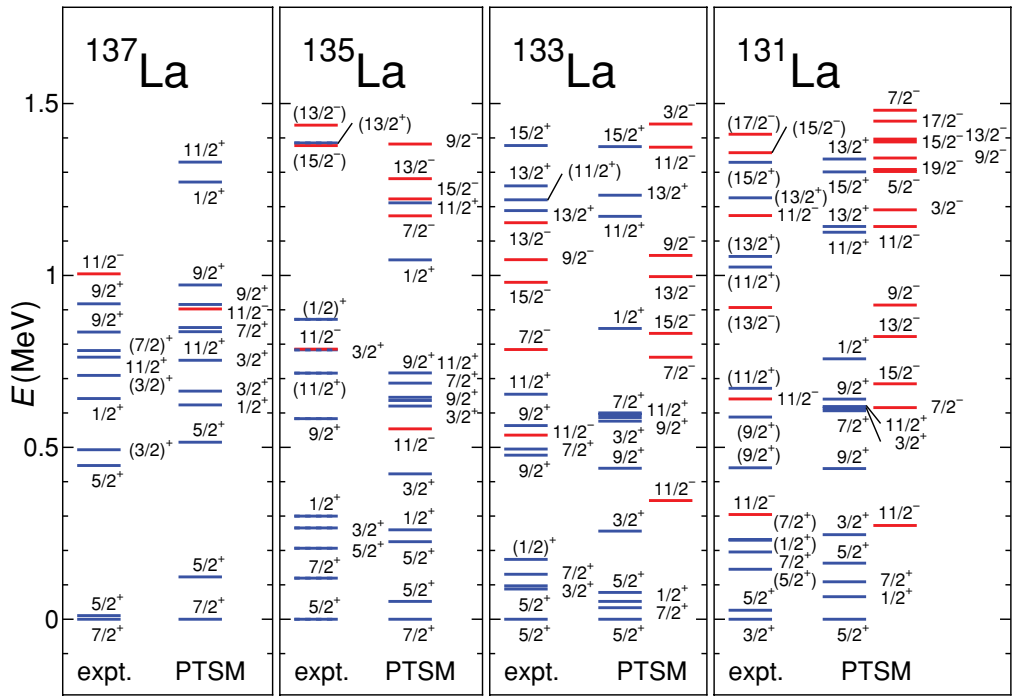

FIG. 11. (Color online) Same as Fig. 7, but for ^{137,135,133,131}La. The experimental data are taken from Refs. [81,83,84,86,92].

the corresponding energy, and the experimental observation is inferred to correspond to this theoretically predicted level. This is confirmed through electromagnetic moments as discussed later. For all the Ce isotopes, the calculation reproduces quite well the experimental energy levels for both the positive- and negative-parity states.

In Fig. 10, the low-lying theoretical energy levels obtained by the PTSM are compared with the experimental data for odd-mass Cs isotopes. For all the nuclei, the PTSM results quite well reproduce the energy levels of the lowest negative-parity states, the $11/2^-_1$ states. This is a direct consequence of the linear change of single-particle energies. In the cases of ^{131}Cs and ^{129}Cs the theoretical energy levels of the second and third excited states with negative parity ($13/2^-_1$ and $15/2^-_1$) come close to the experimental ones.

Concerning the low-lying states with positive parity, the calculated energies agree quite well with experimental ones in ^{135}Cs and ^{133}Cs. The level ordering of the $5/2^+_1$ and $7/2^+_1$ states is predicted in reverse for ^{131}Cs, but their experimental energies are close to one another. For ^{133,131,129}Cs, the experimental energies of the $1/2^+_1$ states smoothly decrease as a function of the number of neutron holes, and the $1/2^+_1$ state becomes the ground state in ^{129}Cs. For all the nuclei, the theoretical $1/2^+_1$ states lie higher in energy than experimental ones, but the decreasing behavior is well simulated by the PTSM. For the other low-lying states, one can find a reasonable one-to-one correspondence between the experimental and theoretical energy levels.

Figure 11 shows the energy spectra of odd-mass La isotopes. For all the nuclei our calculation reproduces the relative positions of the positive- and negative-parity states. Concerning the positive-parity states, there are a few discrepancies between the theoretical energy levels and the experimental data. For example, in ^{135}La, the ordering of the $7/2^+_1$ and $5/2^+_1$ states is predicted in reverse. For the low-lying negative-parity states, good agreements between theoretical energy levels and experimental ones are clearly seen.

TABLE IX. Comparison of the magnetic dipole moments μ (in μ_N) and electric quadrupole moments Q (in e b) obtained by the PTSM (PTSM) with the experiment data (Expt.) for odd-mass Xe, Ba and Ce isotopes. The experimental data are taken from Ref. [79].

Nucleus	I^π_i	μ		Q		Nucleus	I^π_i	μ		Q	
		PTSM	Expt.	PTSM	Expt.			PTSM	Expt.	PTSM	Expt.
^{135}Xe	$1/2^+_1$	−1.25				^{133}Xe	$1/2^+_1$	−0.867			
	$3/2^+_1$	+0.834	+0.9032(7)	+0.187	+0.214(7)		$3/2^+_1$	+0.665	+0.8129(5)	+0.00417	+0.142(5)
	$5/2^+_1$	+1.53		−0.0289			$5/2^+_1$	+0.939		+0.00610	
	$9/2^-_1$	−1.50		+0.292			$9/2^-_1$	−1.32		+0.333	
	$11/2^-_1$	−1.32	−1.1036(14)	+0.292	+0.62(2)		$11/2^-_1$	−1.28	−1.0825(13)	+0.699	+0.77(3)
^{131}Xe	$1/2^+_1$	−0.596				^{129}Xe	$1/2^+_1$	−0.268	−0.777967(8)		
	$3/2^+_1$	+0.398	+0.6915(2)	−0.306	−0.114(1)		$3/2^+_1$	+0.278	+0.58(8)	−0.473	−0.393(10)
	$5/2^+_1$	+0.614		+0.0168			$5/2^+_1$	+0.603		+0.142	
	$9/2^-_1$	−1.14		+0.666			$9/2^-_1$	−1.10		+0.788	
	$11/2^-_1$	−1.25	−0.994(2)	+0.700	+0.73(3)		$11/2^-_1$	−1.13	−0.8906(12)	+0.522	+0.64(2)
^{137}Ba	$1/2^+_1$	−1.26				^{135}Ba	$1/2^+_1$	−0.564			
	$3/2^+_1$	+0.839	+0.93737(2)	+0.201	+0.245(4)		$3/2^+_1$	+0.500	+0.83794(2)	−0.129	+0.160(3)
	$5/2^+_1$	+1.63		−0.107			$5/2^+_1$	+0.815		−0.000902	
	$9/2^-_1$	−1.53		+0.447			$9/2^-_1$	−1.21		+0.355	
	$11/2^-_1$	−1.32	−0.99(3)	+0.482	+0.78(9)		$11/2^-_1$	−1.26	1.001(15)	+0.821	+0.98(8)
^{133}Ba	$1/2^+_1$	−0.425	−0.769(3)			^{131}Ba	$1/2^+_1$	−0.0674	−0.71(2)		
	$3/2^+_1$	+0.273	+0.51(7)	−0.412			$3/2^+_1$	+0.377		−0.551	
	$5/2^+_1$	+0.679		−0.00991			$5/2^+_1$	+0.591		+0.237	
	$9/2^-_1$	−1.12		+0.827			$9/2^-_1$	−1.07	−0.87(2)	+1.07	+1.46(13)
	$11/2^-_1$	−1.22	−0.91(5)	+0.864	+0.89(7)		$11/2^-_1$	−1.00		+0.614	
^{139}Ce	$1/2^+_1$	−1.23				^{137}Ce	$1/2^+_1$	−0.308			
	$3/2^+_1$	+0.862	1.06(4)[a]	+0.244			$3/2^+_1$	+0.269	0.96(4)[a]	−0.316	
	$5/2^+_1$	+1.87		−0.168			$5/2^+_1$	+1.02		−0.0685	
	$9/2^-_1$	−1.60		+0.580			$9/2^-_1$	−1.06		+0.433	
	$11/2^-_1$	−1.30		+0.622			$11/2^-_1$	−1.21	1.01(4)[a]	+1.09	
^{135}Ce	$1/2^+_1$	−0.303				^{133}Ce	$1/2^+_1$	−0.190			
	$3/2^+_1$	+0.255		−0.538			$3/2^+_1$	+0.694		−0.679	
	$5/2^+_1$	+0.918		−0.127			$5/2^+_1$	−0.460		+1.12	
	$9/2^-_1$	−1.08		+1.17			$9/2^-_1$	−1.01		+1.53	
	$11/2^-_1$	−1.15		+1.23			$11/2^-_1$	−0.742		+0.759	

[a]The sign is not given by the measurement.

TABLE X. The same for odd-mass Cs and La isotopes as in Table IX. The experimental data are taken from Ref. [79].

Nucleus	I_i^π	μ		Q		Nucleus	I_i^π	μ		Q	
		PTSM	Expt.	PTSM	Expt.			PTSM	Expt.	PTSM	Expt.
^{135}Cs	$1/2_1^+$	+1.64				^{133}Cs	$1/2_1^+$	+1.85			
	$3/2_1^+$	+1.28		−0.144			$3/2_1^+$	+1.39		−0.136	
	$5/2_1^+$	+2.01		+0.300			$5/2_1^+$	+1.71	+2.0(2)[b]	+0.540	
	$5/2_2^+$	+3.58		−0.433			$5/2_2^+$	+3.74	+3.45(2)[b]	−0.699	−0.33(2)[b]
	$7/2_1^+$	+2.35	+2.7324(2)	+0.130	+0.050(2)		$7/2_1^+$	+2.30	+2.582025(3)	+0.172	−0.00355(4)
	$11/2_1^-$	+6.87		−0.955			$11/2_1^-$	+6.80		−1.25	
^{131}Cs	$1/2_1^+$	+1.96				^{129}Cs	$1/2_1^+$	+1.94	+1.491(8)		
	$3/2_1^+$	+1.15		−0.246			$3/2_1^+$	+0.0432		−0.581	
	$5/2_1^+$	+1.67	+1.86(8)[b]	+0.719	0.022(3)[a,b]		$5/2_1^+$	+1.63		+0.826	
	$5/2_2^+$	+3.53	+3.53(2)[b]	−0.814	−0.575(6)[b]		$5/2_2^+$	+3.24		−0.933	
	$7/2_1^+$	+2.19		+0.196			$7/2_1^+$	+2.05		+0.193	
	$11/2_1^-$	+6.72		−1.48			$11/2_1^-$	+6.63	+6.55(10)	−1.72	
^{137}La	$1/2_1^+$	+1.70				^{135}La	$1/2_1^+$	+1.76			
	$3/2_1^+$	+1.38		−0.0483			$3/2_1^+$	+1.01		−0.232	
	$5/2_1^+$	+3.80		−0.514			$5/2_1^+$	+3.54	+3.70(9)	−0.667	−0.4(4)
	$5/2_2^+$	+1.88		+0.405	+0.24(7)[b]		$5/2_2^+$	+1.91		+0.653	
	$7/2_1^+$	+2.35	+2.700(15)	+0.409	+0.21(3)		$7/2_1^+$	+2.30		+0.456	
	$11/2_1^-$	+6.85		−1.13			$11/2_1^-$	+6.79		−1.37	
^{133}La	$1/2_1^+$	+1.74				^{131}La	$1/2_1^+$	+1.64			
	$3/2_1^+$	+0.482		−0.394			$3/2_1^+$	+0.169		−0.460	
	$5/2_1^+$	+2.08		+0.423			$5/2_1^+$	+1.67		+1.04	
	$5/2_2^+$	+2.99		−0.321			$5/2_2^+$	+2.99		−0.916	
	$7/2_1^+$	+2.21		+0.344			$7/2_1^+$	+2.05		+0.235	
	$11/2_1^-$	+6.72	7.5(5)[a]	−1.57			$11/2_1^-$	+6.66		−1.77	

[a]The sign is not given by the measurement.

[b]The numerals of experimental magnetic moment and quadrupole moments of $5/2_1^-$ states are placed just after the theoretical $5/2_2^-$ state since their theoretical values are very similar to the corresponding experimental values.

B. Magnetic and quadrupole moments

A lot of information about odd-mass nuclear states is obtained through magnetic dipole and electric quadrupole moments. The magnetic dipole and electric quadrupole moments obtained by the PTSM for odd-mass Xe, Ba and Ce isotopes are shown in Table IX together with the experimental data.

We start by discussing the magnetic moments. For Xe and Ba isotopes, the experimental magnetic moments of the $3/2_1^+$ states decrease as the number of valence neutron holes increases. The theoretical magnetic moments of the $3/2_1^+$ states are slightly smaller than the experimental ones. However, their decreasing behavior is also seen in the PTSM results. For the $1/2_1^+$ states, the calculated magnetic moments are smaller than the experimental data in ^{129}Xe and ^{131}Ba. In contrast to the positive-parity states, the absolute values of the calculated magnetic moments for the $11/2_1^-$ states are larger than those for the experimental ones for all the nuclei, but the results are within a reasonable range. The negative values of the magnetic moments indicate that the neutron in the $0h_{11/2}$ orbital gives a dominant contribution to the magnetic moment.

Next let us discuss the quadrupole moments. Our calculations reproduce quite well the observed quadrupole moments except for the $11/2_1^-$ states of ^{135}Xe and ^{137}Ba, which are one-neutron-hole systems. For a reproduction of them, we may need higher-spin pairs such as G pairs. Concerning the $3/2_1^+$ states of Xe isotopes, the experimental quadrupole moments decrease as a function of the number of neutron holes. Our calculation successfully reproduces this decreasing feature of the quadrupole moments of the $3/2_1^+$ states.

In Table X, the calculated magnetic and quadrupole moments for Cs and La isotopes are compared with the experimental data. In ^{133}Cs, ^{131}Cs, and ^{137}La, the level ordering of the $5/2_1^+$ and $5/2_2^+$ states is seemingly predicted in a reverse way in the PTSM, although they are almost degenerate in experiment. By adopting the values of the experimental magnetic moments and quadrupole moments of the $5/2_1^-$ states for the theoretical $5/2_2^-$ states, we find that their theoretical values are very similar to the corresponding experimental values. In ^{135}La the level ordering of these two states seems to be well reproduced, although only the electromagnetic property of the $5/2_1^+$ state is observed experimentally. Concerning other states, the magnetic and quadrupole moments obtained by the PTSM agree well with the experimental ones.

C. $E2$ and $M1$ transition rates

In Tables XI and XII, the theoretical $E2$ and $M1$ transition rates obtained by the PTSM are compared with the

TABLE XI. Comparison of the $B(E2)$ values (in $10^{-2}\ e^2\,\mathrm{b}^2$) and the $B(M1)$ values (in $10^{-2}\mu_N^2$) obtained by the PTSM (PTSM) with the experiment data (Expt.) for ^{131}Xe. The experimental data are taken from Ref. [83].

$I_i^\pi \to I'^\pi_f$	$B(E2)$		$B(M1)$	
	PTSM	Expt.	PTSM	Expt.
$1/2^+_1 \to 3/2^+_1$	0.376	<15	9.78	>5.7
$5/2^+_1 \to 1/2^+_1$	3.98	3.02(9)		
$\to 3/2^+_1$	9.90	11.0(4)	0.307	0.054(5)
$3/2^+_2 \to 5/2^+_1$	1.37		15.4	
$\to 1/2^+_1$	7.26	9.5^{+103}_{-95}	5.13	1.1(9)
$\to 3/2^+_1$	4.00	12(12)	7.37	1.1(11)
$7/2^+_1 \to 3/2^+_2$	< 0.1	0.60(10)		
$\to 5/2^+_1$	< 0.1	0.6(5)	2.55	0.22(1)
$\to 3/2^+_1$	8.32	8.77(75)		
$5/2^+_2 \to 7/2^+_1$	0.406		3.41	
$\to 3/2^+_2$	<0.1	1.6^{+24}_{-16}	0.382	8.4(9)
$\to 5/2^+_1$	0.128		<0.1	
$\to 1/2^+_1$	5.77	10.2(10)		
$\to 3/2^+_1$	2.81	1.9(2)	16.9	16.1(16)
$9/2^-_1 \to 11/2^-_1$	8.91	15(4)	1.13	0.018(7)
$7/2^-_1 \to 9/2^-_1$	2.97	0.07(2)	0.957	0.0915(16)
$\to 11/2^-_1$	10.4	0.1954		
$15/2^-_1 \to 11/2^-_1$	10.5			

TABLE XII. The same as in Table XI for ^{129}Xe. The experimental data are taken from Ref. [82].

$I_i^\pi \to I'^\pi_f$	$B(E2)$		$B(M1)$	
	PTSM	Expt.	PTSM	Expt.
$3/2^+_1 \to 1/2^+_1$	0.596	3(2)	8.50	4.92(18)
$3/2^+_2 \to 3/2^+_1$	1.91	8.40(35)	11.6	0.455(18)
$\to 1/2^+_1$	12.2	2(6)	5.85	0.98(39)
$5/2^+_1 \to 3/2^+_2$	0.213		10.9	
$\to 3/2^+_1$	11.5	22(3)	< 0.1	0.18(2)
$\to 1/2^+_1$	4.31	8.05(81)		
$1/2^+_2 \to 5/2^+_1$	4.14			
$\to 3/2^+_2$	1.88		0.725	0.70(23)
$\to 3/2^+_1$	8.85	2.6(9)	0.319	0.27(9)
$\to 1/2^+_1$			10.0	0.27(9)
$5/2^+_2 \to 1/2^+_2$	0.574			
$\to 5/2^+_1$	0.564		0.0122	
$\to 3/2^+_2$	0.501		0.689	
$\to 3/2^+_1$	4.97		10.2	
$\to 1/2^+_1$	8.66			
$9/2^-_1 \to 11/2^-_1$	18.0		< 0.1	
$7/2^-_1 \to 9/2^-_1$	10.9		0.718	
$\to 11/2^-_1$	4.78			
$15/2^-_1 \to 11/2^-_1$	14.3			

experimental data for ^{131,129}Xe. For the most part, the calculated $B(E2)$ values are in good agreement with the experimental data for ^{131}Xe (see Table XI). It is remarkable that most of the transitions among low-lying states are observed in experiment. The situation for the $E2$ transition rates in ^{129}Xe is similar to that in ^{131}Xe (see Table XII). Several transitions are observed among low-lying states, and agree well with the theoretical results. Concerning the $M1$ transition rates, some transitions are not reproduced well by the PTSM for both ^{131}Xe and ^{129}Xe, since the $M1$ transitions are expected to be very sensitive to the mixing of various single-particle orbitals.

The $E2$ and $M1$ transition rates obtained by the PTSM for ^{133,131}Ba are shown in Table XIII. In experiment, only the $B(E2; 3/2^+_1 \to 1/2^+_1)$ value of $9.5(28) \times 10^{-2} e^2\ \mathrm{b}^2$ and the $B(M1; 3/2^+_1 \to 1/2^+_1)$ value of $2.7(4) \times 10^{-2}\mu_N^2$ are observed for ^{131}Ba.

V. RESULTS FOR DOUBLY ODD NUCLEI

In order to describe doubly odd nuclei, we couple the SD pair plus one-particle states in Eq. (30) in both neutron and proton spaces to the doubly odd state with spin I. The many-body wave function of the doubly odd nucleus is expressed as follows:

$$|\Phi(I\eta)\rangle = [|j_\nu S^{\bar{n}_s} D^{\bar{n}_d}(I_\nu \eta_\nu)\rangle \otimes |j_\pi S^{n_s} D^{n_d}(I_\pi \eta_\pi)\rangle]^{(I)}, \quad (33)$$

where $2(\bar{n}_s + \bar{n}_d) + 1$ and $2(n_s + n_d) + 1$ are the total number of valence neutron holes $\bar{N}_\nu$ and that of valence proton particles N_π, respectively.

A. Energy spectra

In the doubly odd nuclei, the negative-parity states are produced by exciting either a neutron or a proton in a positive-parity orbital into the $0h_{11/2}$ orbital. In the PTSM these neutron and proton excitations are clearly distinguished.

TABLE XIII. The $B(E2)$ values (in $10^{-2}e^2\,\mathrm{b}^2$) and the $B(M1)$ values (in $10^{-2}\mu_N^2$) obtained by the PTSM for ^{133,131}Ba.

$I_i^\pi \to I'^\pi_f$	^{133}Ba		^{131}Ba	
	$B(E2)$	$B(M1)$	$B(E2)$	$B(M1)$
$3/2^+_1 \to 1/2^+_1$	0.342	8.04	3.80	8.54
$3/2^+_2 \to 3/2^+_1$	3.12	8.18	1.63	14.2
$\to 1/2^+_1$	9.89	5.66	13.8	6.48
$5/2^+_1 \to 3/2^+_2$	1.77	9.51	0.205	8.70
$\to 3/2^+_1$	11.6	0.507	10.9	< 0.1
$\to 1/2^+_1$	5.47		3.19	
$1/2^+_2 \to 5/2^+_1$	1.71		7.90	
$\to 3/2^+_2$	< 0.1	< 0.1	6.62	4.68
$\to 3/2^+_1$	9.02	0.739	11.1	< 0.1
$\to 1/2^+_1$		5.27		10.1
$5/2^+_2 \to 1/2^+_2$	0.598		0.258	
$\to 5/2^+_1$	< 0.1	< 0.1	< 0.1	0.407
$\to 3/2^+_2$	0.176	0.709	0.169	0.300
$\to 3/2^+_1$	3.73	14.8	4.36	5.61
$\to 1/2^+_1$	7.75		15.0	
$9/2^-_1 \to 11/2^-_1$	10.8	1.31	25.2	0.667
$7/2^-_1 \to 9/2^-_1$	3.73	2.65	13.2	6.06
$\to 11/2^-_1$	11.0		1.14	
$15/2^-_1 \to 11/2^-_1$	12.2		16.8	
$13/2^-_1 \to 11/2^-_1$	12.4	5.12	14.9	5.08

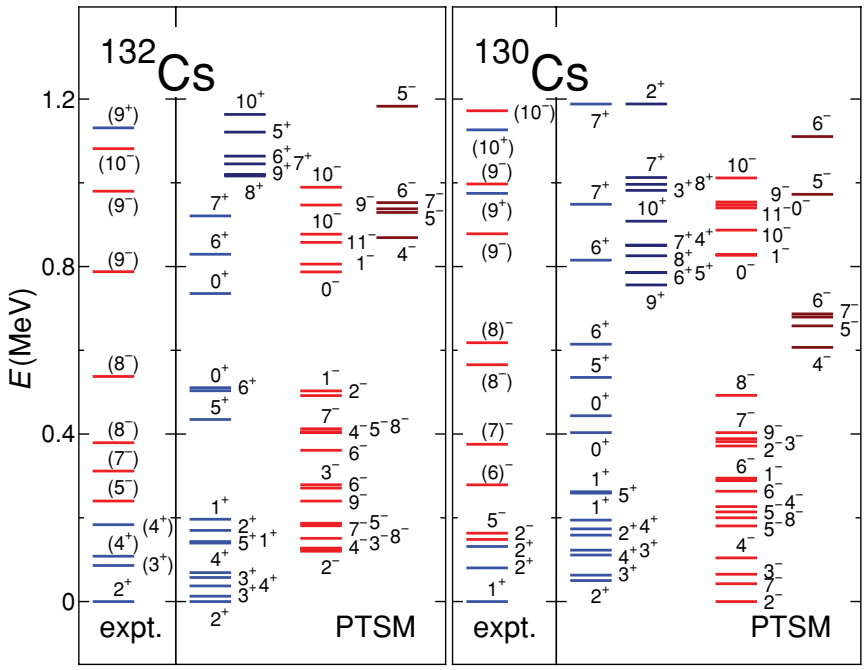

FIG. 12. (Color online) Comparison of the experimental energy levels (expt.) with those of the PTSM (PTSM) for ^{132,130}Cs. The theoretical level sequence of positive-parity states on the left represent the levels built on the valence neutron and proton spaces both with positive parity, and that on the right, both with negative parity. Negative-parity states arising from the valence neutron space are presented on the left-hand side while those from the proton space are shown on the right-hand side. The experimental data are taken from Refs. [93,94].

The experimental energy levels in ^{132}Cs and ^{130}Cs (where available) are shown in comparison with the PTSM calculations in Fig. 12, while those in ^{134}La and ^{132}La are shown in Fig. 13.

In experiment, the ground states are assigned to have positive parity for ^{130}Cs, ^{132}Cs, and ^{134}La, whereas in ^{132}La the ground state is assigned to have negative parity, and the lowest state with positive parity, the $(2)^+_1$ state, has an excitation energy of 155 keV. Concerning ^{132}Cs, ^{134}La, and ^{132}La, calculated energy levels are in good agreement with the experimental data. In particular, the spin and parity of the ground state in each nucleus are reproduced by the PTSM calculation. For ^{130}Cs, the theoretical 1^+_1 state lies higher in energy than the experimental one, but there exists a one-to-one correspondence between the theoretical and experimental levels for the 1^+_1, 2^+_1, 2^+_2 and 2^-_1 states.

Recently, $\Delta I = 1$ doublet bands built on the $\nu h_{11/2} \otimes \pi h_{11/2}$ configuration have been reported in experimental studies of the doubly odd nuclei, ^{132,130}Cs and ^{134,132}La. Their bandhead states of 9^+_1, (9^+_1), and (9^+_1) are experimentally observed at excitation energies of 0.975, 1.131, and 0.775 MeV in ^{130}Cs [95], ^{132}Cs [96], and ^{132}La [97], respectively. In ^{134}La the bandhead position relative to the ground state remains unknown. In the present study, the states with the $\nu h_{11/2} \otimes \pi h_{11/2}$ configuration are produced in the neutron and proton spaces both with negative parity, which are presented

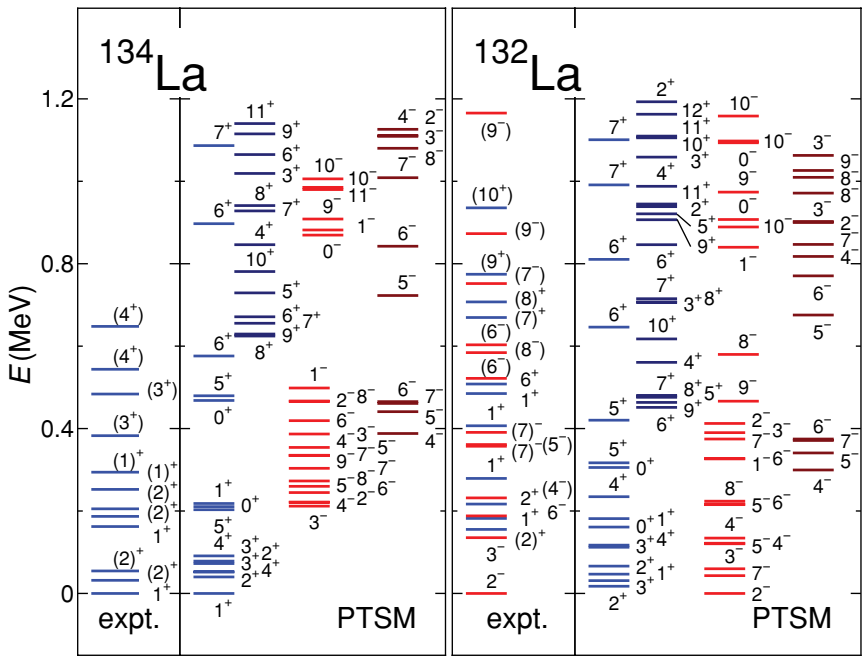

FIG. 13. (Color online) Same as Fig. 12, but for ^{134,132}La. The experimental data are taken from Refs. [50,94].

TABLE XIV. Comparison of the magnetic dipole moments μ (in μ_N) and electric quadrupole moments Q (in e b) obtained by the PTSM (PTSM) with the experiment data (Expt.) for ^{132,130}Cs and ^{134,132}La. The experimental data are taken from Ref. [79].

Nucleus	I_i^π	μ		Q	
		PTSM	Expt.	PTSM	Expt.
^{132}Cs	1_1^+	+0.838		+0.167	
	1_2^+	+2.41		−0.210	
	2_1^+	+2.10	+2.222(7)	+0.523	+0.508(7)
	2_2^+	+1.28		−0.00401	
	9_1^+	+4.57		−0.534	
	2_1^-	−2.34		+0.467	
	3_1^-	−1.97		+0.600	
	5_1^-	−0.474		−0.180	
	5_2^-	−0.651		+1.12	
^{130}Cs	1_1^+	+2.49	+1.460(7)	−0.243	−0.059(6)
	1_2^+	+0.887		+0.119	
	2_1^+	+1.07		+0.650	
	2_2^+	+2.19		+0.489	
	9_1^+	+4.96		−1.03	
	2_1^-	−2.08		+0.598	
	3_1^-	−1.25		−0.0993	
	5_1^-	−0.241		−0.587	
	5_2^-	+0.796	+0.629(4)[a]	+1.17	+1.45(5)[a]
^{134}La	1_1^+	+2.37		−0.215	
	1_2^+	+0.608		+0.222	
	2_1^+	+2.46		+0.156	
	2_2^+	+2.56		−0.131	
	9_1^+	+4.60		−0.518	
	2_1^-	−2.35		+0.585	
	3_1^-	−1.91		+0.641	
	5_1^-	−0.965		+0.688	
	5_2^-	−0.351		+0.430	
^{132}La	1_1^+	+2.23		−0.274	
	1_2^+	+0.186		−0.0322	
	2_1^+	+1.01		+0.794	
	2_2^+	+3.03		−0.558	
	9_1^+	+5.11		−0.929	
	2_1^-	−2.00		+0.801	
	3_1^-	−1.20		−0.104	
	5_1^-	+0.675		+1.35	
	5_2^-	−0.332		−0.414	

[a]The numerals of experimental magnetic and quadrupole moments of the 5_1^- state are placed just after the theoretical 5_2^- state since their values are very similar to experimental values.

on the right-hand side of the positive-parity states in Figs. 12 and 13. The calculated bandhead states lie a bit lower in energy than the experimental ones, but the present results are much better compared to those in the previous study [30–32].

B. Magnetic and quadrupole moments

In Table XIV, calculated magnetic and quadrupole moments for ^{132,130}Cs and ^{134,132}La are compared with the experimental data. Unfortunately, very few experimental studies have been done so far to measure the magnetic dipole and electric quadrupole moments for these nuclei. The PTSM calculation reproduces these moments quite well. We hope that the present study will be helpful for the experimental investigation of the electromagnetic moments on these nuclei in the near future.

VI. SUMMARY

In this paper the level schemes and electromagnetic properties observed in the even-even, odd-mass, and doubly odd nuclei with mass around 130 were investigated in terms of the SD version of the pair-truncated shell model. In this model, the shell model basis is restricted to the SD subspace where the S and D collective pairs are used as the building blocks for even-even nuclei. For a description of odd-mass and doubly odd nuclei, the SD-pair truncation scheme is extended to include unpaired nucleons.

The effective interactions consist of single-particle energies and monopole and quadrupole pairing plus quadrupole-quadrupole interactions, whose strengths are linearly determined as functions of the valence number of nucleons so as to describe the level schemes of even-even and odd-mass nuclei. Energy spectra and $E2$ transition rates for the low-lying collective states were calculated for even-even nuclei, and the results are in excellent agreement with the observation. Calculated relative $B(E2)$ values reproduce very well the experimental data and the results in the O(6) limit of the interacting boson model, which is known to describe γ-unstable nuclei.

For odd-mass nuclei, the linear relation of single-particle energies with valence nucleon numbers results in a great improvement of calculated energies for the corresponding experimental levels; in particular, the relative positions of the positive- and negative-parity states are well reproduced. Electromagnetic moments are also well reproduced by the present calculation. We also applied the same set of interactions to doubly odd nuclei, and excellent agreement is obtained for both energy spectra and electromagnetic moments. In particular, we predict systematically the $\Delta I = 1$ doublet bands built on the $\nu h_{11/2} \otimes \pi h_{11/2}$ configuration. These doublet bands in doubly odd nuclei were investigated extensively in terms of various models. However, most of them could not deal with the Pauli principle explicitly between the even-even part of the nucleus and the fermionic unpaired particles in the $0h_{11/2}$ orbital. Since in the PTSM the basis states are constructed in a subspace of the full shell-model space, the model can treat systematically even-even, odd-mass, and doubly odd nuclei on the equal footing.

In the present approach we investigated the low-lying states for the even-even, odd-mass, and doubly odd nuclei in the mass $A \sim 130$ region using the SD-pair truncation scheme. The description of even-even nuclei was, however, not enough for the anomalous behavior at spin 10. This is due to the backbending phenomena caused by the alignment of two neutrons in the $0h_{11/2}$ orbital. In order to describe these phenomena we need to introduce high-spin pairs made of neutrons in the $0h_{11/2}$ orbital. This extended model was found to reproduce quite well the backbending phenomena of yrast bands and also the nature of 10^+ isomers in this region [27,29]. The systematic study including the high-spin

pairs for the even-even, odd-mass, and doubly odd is now in progress.

ACKNOWLEDGMENTS

The numerical calculations financially supported by Saitama University were carried out partly on the HITACHI SR11000 supercomputers at Supercomputing Division, Information Technology Center, University of Tokyo. This work was supported by a Grant-in-Aid for Scientific Research (C) (No. 20540250) from Japan Society for the Promotion of Science, and by a Grant-in-Aid for Young Scientists (B) (No. 22740171) from The Ministry of Education, Culture, Sports, Science and Technology of Japan.

[1] F. Iachello and A. Arima, *The Interacting Boson Model* (Cambridge University Press, Cambridge, 1987).
[2] S. G. Rohozinski, J. Dobaczewski, B. N. Pomorska, K. Pomorski, and J. Srebrny, Nucl. Phys. A **292**, 66 (1977).
[3] G. Puddu, O. Scholten, and T. Otsuka, Nucl. Phys. A **348**, 109 (1980).
[4] R. F. Casten and P. von Brentano, Phys. Lett. B **152**, 22 (1985).
[5] R. F. Casten, P. von Brentano, K. Heyde, P. Van Isacker, and J. Jolie, Nucl. Phys. A **439**, 289 (1985).
[6] A. Sevrin, K. Heyde, and J. Jolie, Phys. Rev. C **36**, 2631 (1987).
[7] P. von Brentano, A. Gelberg, S. Harissopulos, and R. F. Casten, Phys. Rev. C **38**, 2386 (1988).
[8] X. W. Pan, T. Otsuka, J. Q. Chen, and A. Arima, Phys. Lett. B **287**, 1 (1992).
[9] T. Otsuka, Nucl. Phys. **557**, 531c (1993).
[10] T. Mizusaki and T. Otsuka, Prog. Theor. Phys. Suppl. **125**, 97 (1996).
[11] O. Vogel, P. Van Isacker, A. Gelberg, P. von Brentano, and A. Dewald, Phys. Rev. C **53**, 1660 (1996).
[12] N. V. Zamfir, W.-T. Chou, and R. F. Casten, Phys. Rev. C **57**, 427 (1998).
[13] F. Iachello and P. Van Isacker, *The Interacting Boson-Fermion Model* (Cambridge University Press, Cambridge, 1991).
[14] M. A. Cunningham, Nucl. Phys. A **385**, 204 (1982).
[15] M. A. Cunningham, Nucl. Phys. A **385**, 221 (1982).
[16] J. M. Arias, C. E. Alonso, and R. Bijker, Nucl. Phys. A **445**, 33 (1985).
[17] C. E. Alonso, J. M. Arias, and M. Lozano, J. Phys. G **13**, 1269 (1987).
[18] H. C. Chiang, S. T. Hsieh, and D. S. Chuu, Phys. Rev. C **39**, 2390 (1989).
[19] S. T. Hsieh, H. C. Chiang, and M. M. King Yen, Phys. Rev. C **41**, 2898 (1990).
[20] D. Bucurescu, G. Cata-Danil, N. V. Zamfir, A. Gizon, and J. Gizon, Phys. Rev. C **43**, 2610 (1991).
[21] N. Yoshida, A. Gelberg, T. Otsuka, I. Wiedenhover, H. Sagawa, and P. von Brentano, Nucl. Phys. A **619**, 65 (1997).
[22] N. Yoshinaga, Nucl. Phys. A **503**, 65 (1989).
[23] N. Yoshinaga and D. M. Brink, Nucl. Phys. A **515**, 1 (1990).
[24] N. Yoshinaga, Nucl. Phys. A **570**, 421 (1994).
[25] N. Yoshinaga, T. Mizusaki, A. Arima, and Y. D. Devi, Prog. Theor. Phys. Suppl. **125**, 65 (1996).
[26] N. Yoshinaga, Y. D. Devi, and A. Arima, Phys. Rev. C **62**, 024309 (2000).
[27] K. Higashiyama, N. Yoshinaga, and K. Tanabe, Phys. Rev. C **67**, 044305 (2003).
[28] N. Yoshinaga and K. Higashiyama, Phys. Rev. C **69**, 054309 (2004).
[29] T. Takahashi, N. Yoshinaga, and K. Higashiyama, Phys. Rev. C **71**, 014305 (2005).
[30] K. Higashiyama and N. Yoshinaga, Prog. Theor. Phys. **113**, 1139 (2005).
[31] K. Higashiyama, N. Yoshinaga, and K. Tanabe, Phys. Rev. C **72**, 024315 (2005).
[32] N. Yoshinaga and K. Higashiyama, J. Phys. G **31**, S1455 (2005).
[33] N. Yoshinaga and K. Higashiyama, Eur. Phys. J. A **30**, 343 (2006); **31**, 395 (2007).
[34] K. Higashiyama and N. Yoshinaga, Eur. Phys. J. A **33**, 355 (2007).
[35] K. Higashiyama and N. Yoshinaga, Prog. Theor. Phys. **120**, 525 (2008).
[36] N. Yoshinaga and K. Higashiyama, J. Phys. G **37**, 115104 (2010).
[37] B. Fogelberg and J. Blomqvist, Nucl. Phys. A **429**, 205 (1984).
[38] M. Sanchez-Vega, B. Fogelberg, H. Mach, R. B. E. Taylor, A. Lindroth, J. Blomqvist, A. Covello, and A. Gargano, Phys. Rev. C **60**, 024303 (1999).
[39] W. J. Baldridge, Phys. Rev. C **18**, 530 (1978).
[40] L. Goettig, C. Droste, A. Dygo, T. Morek, J. S. R. Broda, J. Styczeń, H. H. J. Hattula, and M. Jääskeläinen, Nucl. Phys. A **357**, 109 (1981).
[41] J. Srebrny *et al.*, Nucl. Phys. A **557**, 663c (1993).
[42] S. Juutinen *et al.*, Phys. Rev. C **52**, 2946 (1995).
[43] R. Kühn, K. Kirch, I. Wiedenhöver, O. Vogel, M. Wilhelm, U. Neuneyer, M. Luig, A. Gelberg, and P. von Brentano, Nucl. Phys. A **597**, 85 (1996).
[44] A. Gade, I. Wiedenhöver, H. Meise, A. Gelberg, and P. von Brentano, Nucl. Phys. A **697**, 75 (2002).
[45] J. N. Orce *et al.*, Phys. Rev. C **74**, 034318 (2006).
[46] L. Coquard *et al.*, Phys. Rev. C **80**, 061304(R) (2009).
[47] W. Gelletly, W. R. Kane, and D. R. MacKenzie, Phys. Rev. C **9**, 2363 (1974).
[48] C. Girit, W. D. Hamilton, and E. Michelakakis, J. Phys. G **6**, 1025 (1980).
[49] J. Genevey, J. A. Pinston, C. Foin, M. Rejmund, R. F. Casten, H. Faust, and S. Oberstedt, Phys. Rev. C **63**, 054315 (2001).
[50] A. A. Sonzogni, Nucl. Data Sheets **103**, 1 (2004).
[51] A. Gade, I. Wiedenhöver, J. Gableske, A. Gelberg, H. Meise, N. Pietralla, and P. von Brentano, Nucl. Phys. A **665**, 268 (2000).
[52] T. Morek, H. Beuscher, B. Bochev, D. R. Haenni, R. M. Lieder, T. Kutsarova, M. Muller-Veggian, and A. Neskakis, Z. Phys. A **298**, 267 (1980).
[53] D. Bazzacco, W. Gast, A. Gelberg, U. Kaup, K. Schiffer, A. Dewald, R. Reinhardt, K. O. Zell, and P. von Brentano, Nucl. Phys. A **436**, 506 (1985).
[54] B. Fazekas, T. Belgya, G. Molnár, A. Veres, R. A. Gatenby, S. W. Yates, and T. Otsuka, Nucl. Phys. A **548**, 249 (1992).
[55] K. Kirch, G. Siems, M. Eschenauer, A. Gelberg, A. M. R. Kühn a, U. Neuneyer, O. Vogel, I. Wiedenhöver, P. von Brentano, and T. Otsuka, Nucl. Phys. A **587**, 211 (1995).

[56] O. Vogel *et al.*, Eur. Phys. J. A **4**, 323 (1999).
[57] A. Wolf *et al.*, Phys. Rev. C **66**, 024323 (2002).
[58] J. J. Valiente-Dobón *et al.*, Phys. Rev. C **69**, 024316 (2004).
[59] S. Mukhopadhyay, M. Scheck, B. Crider, S. N. Choudry, E. Elhami, E. Peters, M. T. McEllistrem, J. N. Orce, and S. W. Yates, Phys. Rev. C **78**, 034317 (2008).
[60] B. H. Ketelle, A. R. Brosi, and J. R. Van Hise, Phys. Rev. C **4**, 1431 (1971).
[61] D. M. Todd, R. Aryaeinejad, D. J. G. Love, A. H. Nelson, P. J. Nolan, P. J. Smith, and P. J. Twin, J. Phys. G **10**, 1407 (1984).
[62] G. Lo Bianco, P. Paruzzi, K. P. Schmittgen, R. Reinhardt, A. Gelberg, K. O. Zell, P. Von Brentano, and N. Blasi, Nucl. Phys. A **470**, 266 (1987).
[63] T. Murakami, Y. Gono, M. Oshima, H. Kusakari, K. Morita, A. Yoshida, and H. Kumagai, J. Phys. Soc. Jpn. **4**, 1431 (1971).
[64] E. S. Paul *et al.*, Nucl. Phys. A **619**, 177 (1997).
[65] A. Gade *et al.*, Nucl. Phys. A **643**, 225 (1998).
[66] A. Gade, I. Wiedenhöver, M. Luig, A. Gelberg, H. Meise, N. Pietralla, V. Werner, and P. von Brentano, Nucl. Phys. A **673**, 45 (2000).
[67] E. S. Paul, C. W. Beausang, D. B. Fossan, R. Ma, W. F. Piel Jr., P. K. Weng, and N. Xu, Phys. Rev. C **36**, 153 (1987).
[68] M. O. Kortelahti, B. D. Kern, R. A. Braga, R. W. Fink, I. C. Girit, and R. L. Mlekodaj, Phys. Rev. C **42**, 1267 (1990).
[69] G. de Angelis *et al.*, Phys. Rev. C **49**, 2990 (1994).
[70] C. M. Petrache *et al.*, Phys. Lett. B **415**, 223 (1997).
[71] T. Klemme *et al.*, Phys. Rev. C **60**, 034301 (1999).
[72] E. Williams *et al.*, Phys. Rev. C **80**, 054309 (2009).
[73] K. A. Gladnishki *et al.*, Phys. Rev. C **82**, 037302 (2010).
[74] A. Bohr and B. Mottelson, *Nuclear Structure*, Vol. 1 (Benjamin, New York, 1975).
[75] S. Raman, C. W. Nestor Jr., and P. Tikkanen, At. Data Nucl. Data Tables **78**, 1 (2001).
[76] A. M. Kleinfeld, A. Bockisch, and K. P. Lieb, Nucl. Phys. A **283**, 526 (1977).
[77] L. Coquard *et al.*, Phys. Rev. C **82**, 024317 (2010).
[78] K. Sieja, G. Martínez-Pinedo, L. Coquard, and N. Pietralla, Phys. Rev. C **80**, 054311 (2009).
[79] N. J. Stone, At. Data Nucl. Data Tables **90**, 75 (2005).
[80] Z. Zhao, J. Yan, A. Gelberg, R. Reinhardt, W. Lieberz, A. Dewald, R. Wirowski, K. O. Zell, and P. von Brentano, Z. Phys. A **331**, 113 (1988).
[81] S. Rab, Nucl. Data Sheets **75**, 491 (1995).
[82] Y. Tendow, Nucl. Data Sheets **77**, 631 (1996).
[83] Yu. Khazov, I. Mitropolsky, and A. Rodionov, Nucl. Data Sheets **107**, 2715 (2006).
[84] B. Singh, A. A. Rodionov, and Y. L. Khazov, Nucl. Data Sheets **109**, 517 (2008).
[85] M. S. Fetea *et al.*, Phys. Rev. C **73**, 051301(R) (2006).
[86] E. Browne and J. K. Tuli, Nucl. Data Sheets **108**, 2173 (2007).
[87] G. Suliman *et al.*, Eur. Phys. J. A **41**, 299 (2009).
[88] G. Suliman *et al.*, Eur. Phys. J. A **46**, 187 (2010).
[89] D. Bucurescua, G. Căta-Danil, I. Căta-Danil, M. Ivaşcu, N. Marginean, R. Marginean, L. C. Mihăilescu, C. Rusu, and G. Suliman, Eur. Phys. J. A **27**, 301 (2006).
[90] R. Kumar, K. Singh, D. Mehta, N. Singh, S. S. Malik, E. S. Paul, A. Görgen, S. Chmel, R. P. Singh, and S. Muralithar, Eur. Phys. J. A **24**, 13 (2005).
[91] S. Sihotra *et al.*, Phys. Rev. C **79**, 044317 (2009).
[92] S. Chanda *et al.*, Nucl. Phys. A **775**, 153 (2006).
[93] B. Singh, Nucl. Data Sheets **93**, 33 (2001).
[94] Y. Khazov, A. A. Rodionov, S. Sakharov, and B. Singh, Nucl. Data Sheets **104**, 497 (2005).
[95] P. R. Sala, N. Blasi, G. Lo Bianco, A. Mazzoleni, R. Reinhardt, K. Schiffer, K. P. Schmittgen, G. Siems, and P. von Brentano, Nucl. Phys. A **531**, 383 (1991).
[96] T. Hayakawa *et al.*, Z. Phys. A **357**, 349 (1997).
[97] V. Kumar, P. Das, R. P. Singh, S. Muralithar, and R. K. Bhowmik, Eur. Phys. J. A **17**, 153 (2003).